Magnetization of 0-26.5 Ma seafloor at the ultraslow spreading Southwest Indian Ridge, 61°-67°E

Daniel Sauter, Mathilde Cannat, Véronique Mendel

HAL Id: insu-01827673

https://insu.hal.science/insu-01827673

Submitted on 2 Jul 2018

Geochemistry Geophysics Geosystems G³

AN ELECTRONIC JOURNAL OF THE EARTH SCIENCES

Published by AGU and the Geochemical Society

Magnetization of 0–26.5 Ma seafloor at the ultraslow spreading Southwest Indian Ridge, 61°–67°E

Daniel Sauter

Institut de Physique du Globe de Strasbourg, UMR7516 CNRS-ULP, Ecole et Observatoire des Sciences de la Terre, 5 Rue Descartes, F-67084 Strasbourg CEDEX, France (daniel.sauter@eost.u-strasbg.fr)

Mathilde Cannat

Equipe de Géosciences Marines, CNRS-UMR7097, Institut de Physique du Globe, 4 Place Jussieu, F-75252 Paris CEDEX 05, France (cannat@ipgp.jussieu.fr)

Véronique Mendel

Institut de Physique du Globe de Strasbourg, UMR7516 CNRS-ULP, Ecole et Observatoire des Sciences de la Terre, 5 Rue Descartes, F-67084 Strasbourg CEDEX, France (veronique.mendel@eost.u-strasbg.fr)

[1] We investigate the magnetic signature of volcanic and nonvolcanic seafloor areas along the Southwest Indian Ridge between 61°E and 67°E and analyze their relationship with crustal thickness variations and past to present ridge segmentation. This part of the Southwest Indian Ridge is an end-member for the global ridge system in terms of low melt supply, thin crust, and ultraslow spreading rates. It is characterized by large expanses of seafloor that show no evidence for a volcanic upper crustal layer. We find that variations of intrinsic magnetization and thickness of the basaltic extrusive layer, where it is present, dominate the present-day along-axis crustal magnetization. Off-axis, the magnetization contrast is on average higher for volcanic seafloor than for smooth nonvolcanic topography, indicating that the contribution of the basaltic upper crustal layer to the production of magnetic anomalies remains important. However, magnetic anomalies that record past magnetic polarity events are found almost everywhere in the survey area, even over domains that lack a volcanic upper crustal layer, arguing thus for the contribution of other sources. We propose that both gabbros and serpentinized peridotites contribute to these anomalies. Although not systematic, and weak over most parts of the survey area, an induced component of magnetization is clearly present in some nonvolcanic seafloor domains. Serpentinized peridotites are the likely carriers of this induced magnetization component.

1. Introduction

[2] The Southwest Indian Ridge (SWIR), separating Africa and Antarctica, is among the world's slowest spreading ridges with a full spreading rate of ∼14 km/Ma at 64°E/28°S [Horner-Johnson et al., 2005; Patriat et al., 1997]. The ultraslow spreading ridges (mainly the SWIR and the Arctic ridges with 8–13 km/Ma spreading rates) make up a significant proportion (∼10%) of the global oceanic ridge system. High-resolution mapping and sampling of the SWIR and the Arctic ridges were accomplished only in the late 1990s [Cannat et al., 1999; Hosford et al., 2003; Mendel et al., 2003; Meyzen et al., 2003, 2005; Michael et al., 2003; Patriat et al., 1997; Sauter et al., 2001; Seyler et al., 2003]. Up to now investigations of these ridges consist mainly of along-axis surveys revealing that large expanses of mantle-derived peridotites are exposed at the seafloor which led to the suggestion that ultraslow spreading ridges may be amagmatic over long portions of the axis [Dick et al., 2003; Sauter et al., 2004b].

[3] The conventional understanding of seafloor magnetic anomalies is that their source mainly resides in an upper crustal layer of effusive volcanics [Harrison, 1987]. Studies at slow spreading ridges, however, have also suggested a contribution from other lithologies, such as gabbros and serpentinized peridotites [Nazarova, 1994; Pariso and Johnson, 1993; Oufi et al., 2002], which are locally exhumed along axial normal faults [Lagabrielle et al., 1998]. Hosford et al. [2003] have proposed that such tectonically exhumed rocks are responsible for magnetic anomalies measured over the off-axis traces of axial discontinuities and segment ends near 57°E along the SWIR. Our study area (Figure 1) displays the widest expanses known to date of seafloor with no evidence for a volcanic upper crustal layer. Recently acquired multibeam bathymetric data revealed that a significant proportion (∼37%) of the axial and off-axis seafloor generated in our study area shows no evidence for a volcanic upper crustal layer [Cannat et al., 2006] (Figure 2). This nonvolcanic ocean floor has no equivalent at faster spreading ridges and has been called "smooth seafloor" because it occurs in the form of broad ridges, with a smooth, rounded topography [Cannat et al., 2006]. It shows no resolvable volcanic cones on bathymetric data [Cannat et al., 2006; Sauter et al., 2004b]. When sampled by dredging, smooth seafloor terranes have yielded serpentinized mantle-derived peridotites, with minor basalts and gabbros [Seyler et al.,

2003]. Seafloor with unambiguous volcanic features represents ∼59% of the mapped area. Corrugated surfaces, similar to those described at faster ridges and interpreted as exhumed detachment fault surfaces [Cann et al., 1997; Tucholke et al., 1998], represent 4% of the mapped area. The off-axis distribution of the volcanic, corrugated, and smooth, nonvolcanic seafloor, their gravity signature, and their possible modes of formation have been addressed by Cannat et al. [2006].

[4] In this paper we investigate the magnetic signature of the volcanic and nonvolcanic seafloor and their relationship with crustal thickness variations and past to present ridge segmentation recorded in our study area. We then discuss the processes that may control the magnetic structure of ultraslow spreading ridges and propose hypotheses for the nature of the source of marine magnetic anomalies at those ridges. We use an extensive off-axis data set covering ∼200,000 km² (about twice the area of Iceland) and extending up to ∼26.5 Ma old crust in the easternmost part of the SWIR [Cannat et al., 2006]. Both the very deep setting of the axis and the $Na_{8.0}$ content of the basaltic glasses suggest that this easternmost part of the SWIR represents a melt poor end-member for the ultraslow SWIR [Cannat et al., 1999; Robinson et al., 2001]. Gravity and seismic data show that the melt supply in this area is on average lower, more focused and shorter lived than at the faster spreading Mid-Atlantic Ridge (MAR) [Cannat et al., 2003; Muller et al., 1999].

2. SWIR East of the Melville Fracture Zone: A Melt-Poor Section of an Ultraslow Spreading Ridge

[5] Although the spreading rate of the SWIR is almost constant from the Andrew Bain FZ (fracture zone; 32°E) to the Rodrigues Triple Junction (RTJ; 70°E) [Horner-Johnson et al., 2005], marked changes of segmentation style and mean axial depth occur across the Gallieni and Melville FZs (52°15′E and 60°45′E, respectively) [Mendel et al., 1997; Sauter et al., 2001]. Mean axial depths increase eastward from 3090 m between 49°E and the Gallieni FZ, to 4730 m in the deepest part of the ridge, between the Melville FZ and 69°E close to the RTJ [Cannat et al., 1999]. This large scale variation of axial depths suggests that the regional density structure of the axial region also varies, the deepest ridge section to the east of the Melville FZ being underlain by thinner crust and/or
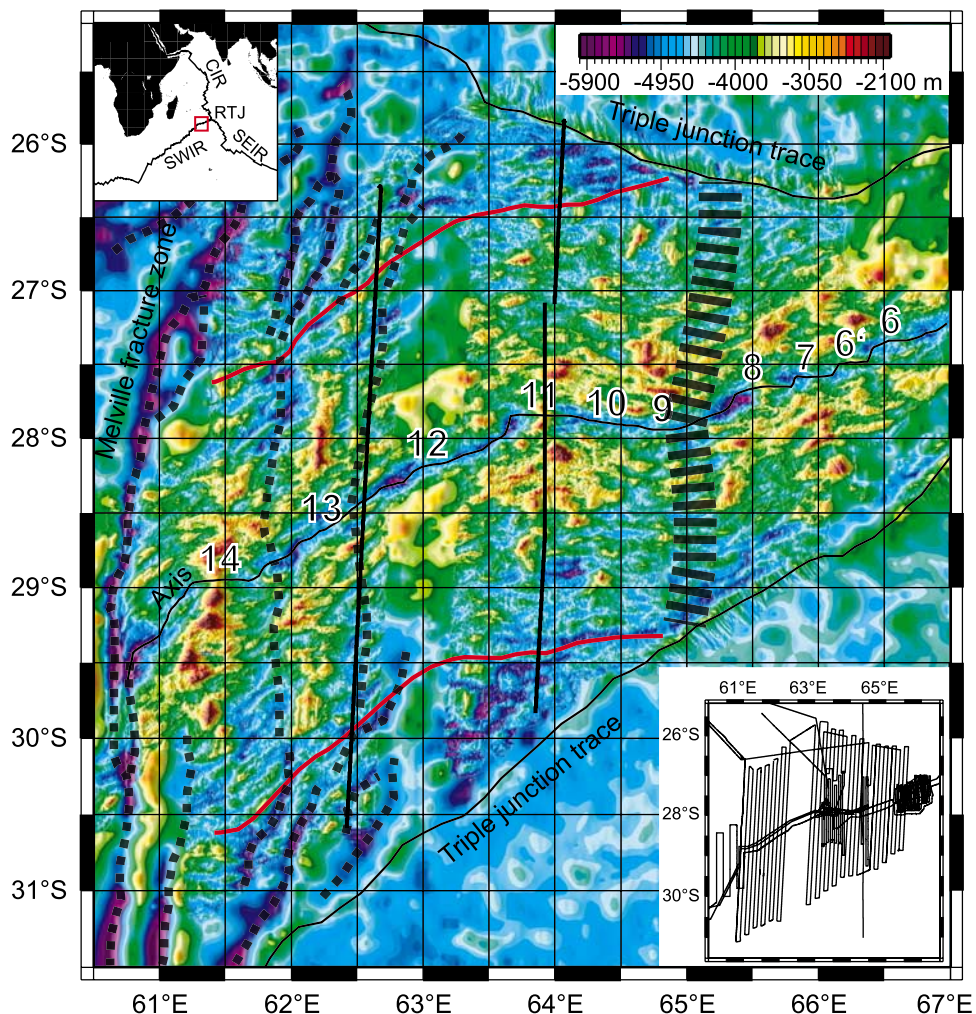
Figure 1. Bathymetric map of the Southwest Indian Ridge (SWIR) between 61°E and 67°E obtained by merging the multibeam bathymetric data collected during "SWIR61-65" [*Cannat et al.*, 2006], "Indoyo" [*Cannat et al.*, 2003], "Capsing" [*Patriat et al.*, 1997], and "Rodrigues" [*Munschy and Schlich*, 1990] cruises and satellite-derived bathymetry [*Smith and Sandwell*, 1997] outside the survey areas. Dashed black lines indicate the Melville fracture zone and the traces of axial discontinuities. Closely spaced horizontal dashes between 65° and 65°30′E show a broad and slightly V-shaped region with mainly nonvolcanic seafloor and on average higher Residual Mantle Bouguer gravity Anomalies (RMBA) (see text for further explanations). The ridge axis and the triple junction traces are drawn in black. The red line indicates the C6C isochron (~24 Ma). The near N-S thin black lines indicate profiles shown in Figure 12. Numbers indicate the segments cited in the text and in other figures following the nomenclature of *Cannat et al.* [1999]. The bottom right inset shows the cruise tracks used in this study. SEIR, Southeast Indian Ridge; CIR, Central Indian Ridge; RTJ, Rodrigues Triple Junction.

colder mantle. Anomalously thin crust (average crustal thickness of 3.7 km) in the Melville FZ - RTJ region is also indicated by seismic profiles acquired at 66°E [*Muller et al.*, 1999]. This is consistent with along-axis variation of geochemical indicators of the extent of mantle partial melting (such as the $Na_{8.0}$ content of basaltic glasses, and the chromium content of spinel in abyssal peridotites) between 49°E and 70°E [*Meyzen et al.*, 2003] [*Seyler et al.*, 2003]. The geochemistry of both the basalts and the peridotites to the east of the Mel-

ville FZ also argues for a strongly heterogeneous mantle source composition [*Meyzen et al.*, 2003; *Seyler et al.*, 2003]. Three-dimensional S-wave velocity models of the upper 100 km in the Indian Ocean reveal a positive anomaly of S-wave velocities which is consistent with a colder and thus denser mantle beneath the easternmost section of the SWIR [*Debayle and Lévêque*, 1997]. Regional axial depths, seismic data, geochemical proxies for the extent of partial melting and tomographic images therefore concur in indicating that the
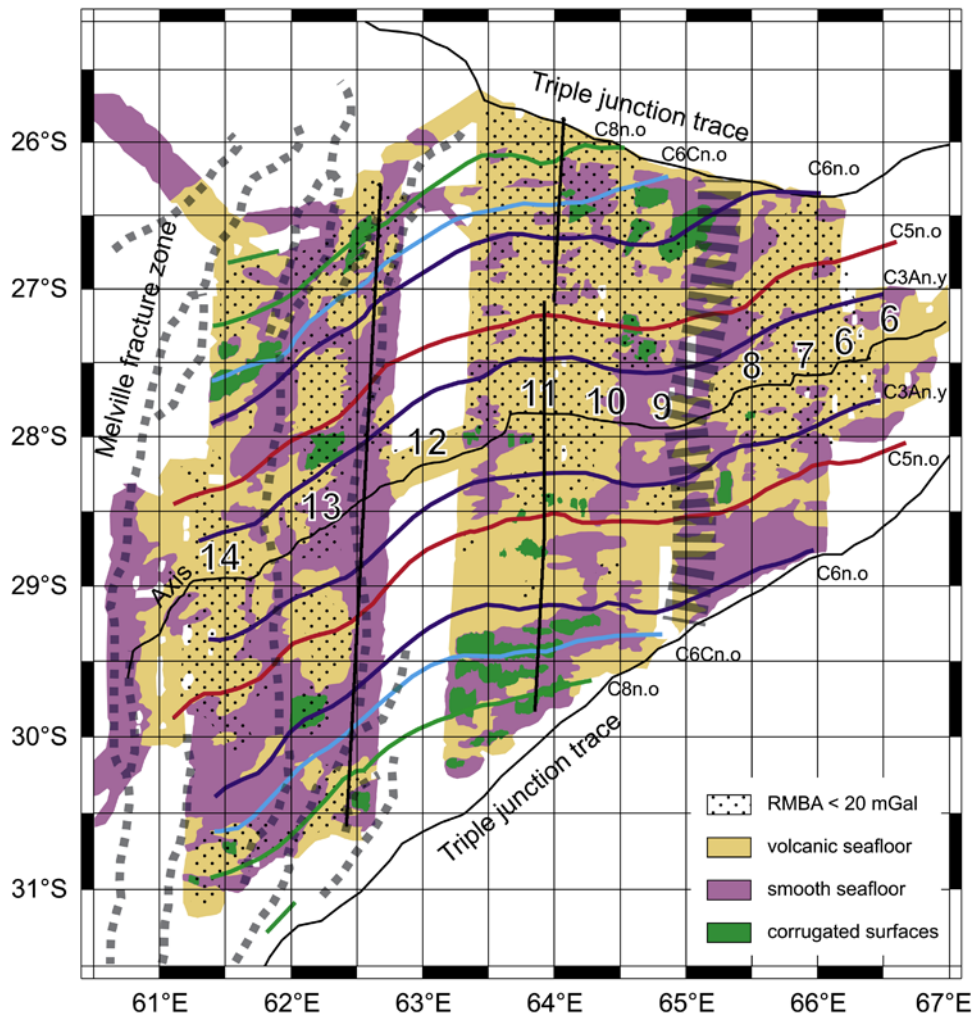
Figure 2. Map of seafloor morphologies at the Southwest Indian Ridge (SWIR) between 61°E and 67°E [after *Cannat et al.*, 2006]. Grey dashed lines indicate axial discontinuities. Three different types of seafloor morphologies were identified [*Cannat et al.*, 2006]: corrugated surfaces, volcanic seafloor (displaying unambiguous volcanic features such as volcanic cones), and smooth seafloor occurring in the form of broad ridges, with a smooth, rounded topography and no resolvable volcanic cone. Dotted areas correspond to domains of Residual Mantle Bouguer gravity Anomalies (RMBA) < 20 mGal (inferred thick crust areas). Isochrons are drawn following the identification of magnetic anomalies of *Cannat et al.* [2006] using the geomagnetic reversal timescale of *Cande and Kent* [1995]: C3An.y (5.894 Ma), C5n.o (10.949 Ma), C6n.o (20.131 Ma), C6Cn.o (24.118 Ma), C8n.o (26.554 Ma), and C11n.y (29.401 Ma) (y and o stand for the young and old edges of the magnetic block, respectively). The near N-S thin black lines indicate profiles shown in Figure 12.

section of the SWIR between the Melville FZ and the RTJ has an anomalously low melt supply.

3. Processing of Magnetic Data

[6] The majority of the data used in this study derive from the "SWIR 61–65" cruise on board the French R/V *Marion Dufresne* in October 2003. Track lines were oriented N03°E (parallel to the mean spreading direction for the last 11 Ma

[*Lemaux et al.*, 2002]), spaced every ∼6 nm and extending up to ∼26.5 Ma old crust (Figure 1). Multibeam bathymetry, magnetics and gravity were collected together with GPS navigation. These data were merged with existing off-axis data from earlier cruises: the "Rodrigues" cruises in 1984 between 65°45′E and 66°45′E [*Munschy and Schlich*, 1990; *Wang and Cochran*, 1995], the "Capsing" cruise in 1993 close to the Melville FZ [*Patriat et al.*, 1997], the "Indoyo" cruise in

1998 between 64°E and 65°E [*Cannat et al.*, 2003], the "FUJI" cruise in 1997 along the axis [*Sauter et al.*, 2002] and several transit cruises which pass through the survey area with oblique routes (Figure 1). The processing of the bathymetric and gravimetric data is described in [*Cannat et al.*, 2006].

[7] During the "SWIR 61–65," "Rodrigues," "Capsing," "Indoyo" and "FUJI" cruises, total magnetic field data were collected using towed proton precession magnetometers. These data were corrected for the regional magnetic field using the definitive geomagnetic reference field (IGRF 10th generation) [*Maus et al.*, 2005]. After applying constant offsets to the data of the earlier cruises, the mean of the absolute value of the magnetic anomaly differences for 896 cross-over points was 13 nT with a standard deviation of 11 nT. We interpolated magnetic anomaly values between the ship tracks using a minimum curvature algorithm [*Smith and Wessel*, 1990] with a tension factor of 0.25 on an anisotropic grid. Since the magnetic data of the "SWIR 61–65" cruise are averaged over 1 minute, we have data every ∼0.2 nm (at 13.5 knots) along the ship tracks that are spaced every ∼6 nm. We therefore created magnetic anomaly and bathymetry grids with many nodes along-track (every 0.5 nm) and fewer across-track (every 2 nm) mimicking the data distribution. This technique attempts to minimize the loss of the shorter wavelength signals and to better retain amplitude information needed to understand crustal magnetization patterns. The grids were then resampled at 1 nm (Figure 3a).

[8] A three-dimensional inversion for crustal magnetization was performed to account for the distorting effects of seafloor topography and skewness. We used the Fourier technique of *Parker and Huestis* [1974] and extended for grid analysis by *Macdonald et al.* [1980] assuming a source layer of constant thickness (0.5 km) and an upper boundary defined by the bathymetry. This inversion emphasizes lateral variations in crustal magnetization but cannot discriminate between changes in source thickness and changes in source intensity. We assumed a direction of magnetization that corresponds to a geocentric axial dipole and mirrored both the bathymetric and magnetic anomaly input grids to minimize the edge effects of the Fourier transform. To ensure convergence during the inversion, we employed cosine tapered bandpass filters with long- and short-wavelength cutoffs of 700 km and 3.5 km. As the magnetization

solution is more or less balanced over the Brunhes/Matuyama reversal, no annihilator has been added to this solution which is shown in Figure 3b.

4. Spreading Rates and Opening Directions

[9] Magnetic anomalies were identified along the profiles of the "SWIR61-65" cruise by *Cannat et al.* [2006] and by *Patriat et al.* [2008] along profiles of earlier cruises from the Andrew Bain FZ to the RTJ. These anomaly identifications revealed that the spreading rate and direction have been almost constant (13.5 km/Ma and N0.2°E on average in our survey area) for the last 20 Ma. These results agree with spreading rate calculations by *Hosford et al.* [2003], who found a mean 14 km/Ma spreading rate for the last 18 Ma to the west of our study area (between the Atlantis II and Novara FZs). Before ∼24 Ma (anomaly C6Cn.o) the spreading rate was two times higher (∼30 km/Ma [*Patriat et al.*, 2008]). A small 10–15° counter clockwise change of spreading direction accompanied this change of spreading rate.

5. Ridge Segmentation Record

5.1. Present-Day Segmentation

[10] The segmentation pattern varies markedly on either side of the Melville FZ. Between the Gallieni and Melville FZs, ∼50-km-long spreading segments occur regularly, alternating with melt-poor nontransform discontinuities which are often longer than the segments themselves [*Sauter et al.*, 2001]. By contrast, the segmentation pattern is highly variable east of the Melville FZ. The most striking features in this deepest part of the SWIR are three elevated segments (from west to east 14, 11 and 8, following the nomenclature of *Cannat et al.* [1999]) with an along-axis relief up to 2600 m [*Mendel et al.*, 1997]. Moderate to large variations of the Residual Mantle Bouguer gravity Anomalies (RMBA) have been observed between the center and ends of these spreading segments [*Cannat et al.*, 1999] suggesting differences in crustal thickness of up to 5 km along-axis [*Cannat et al.*, 2003]. Seafloor morphology [*Cannat et al.*, 2006; *Mendel and Sauter*, 1997; *Mendel et al.*, 1997], side-scan sonar mapping [*Sauter et al.*, 2004b] and submersible studies [*Fujimoto et al.*, 1999] show that these high-relief segments correspond to large volcanic constructions that almost fill the axial valley at the
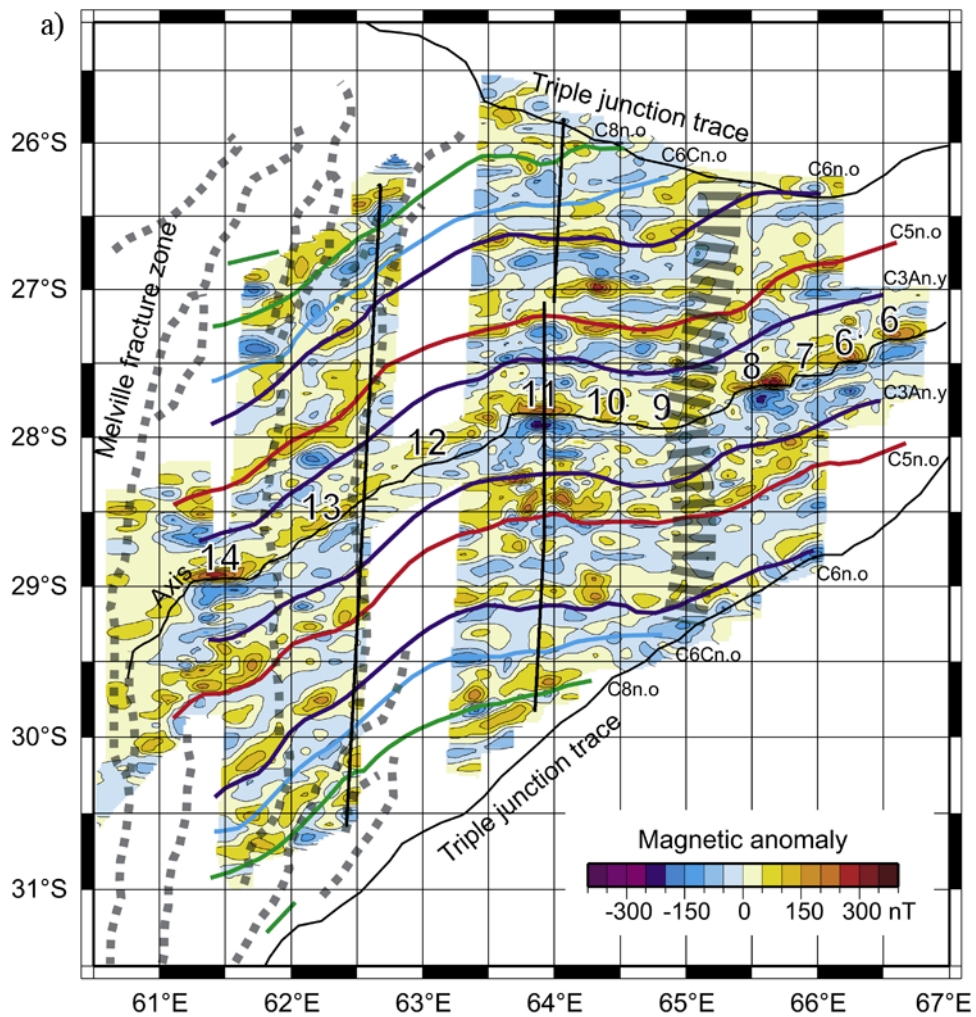
Figure 3. (a) Magnetic anomaly map and (b) crustal magnetization map. The color and contour intervals of the magnetic anomaly map are 50 nT. The color intervals of the magnetization map are 2 A/m. The magnetization distribution is calculated by a three-dimensional inversion of the magnetic anomaly map with a constant-thickness source layer of 0.5 km whose upper surface is defined by the bathymetry (see text for further details). The SWIR axis and isochrons are as in Figure 2. The near N-S thin black lines indicate profiles shown in Figure 12.

segment centers. These volcanic constructions are significantly larger than the neovolcanic ridges that have been described at the MAR [*Smith and Cann*, 1999], but could be similar to volcanic features described at the ultraslow spreading Gakkel and Knipovitch Ridges in the Arctic [*Cochran et al.*, 2003; *Okino et al.*, 2002].

[11] Smaller bathymetric swells (relief < 1300 m) crowned by axial volcanic ridges with fresh-looking volcanics [*Sauter et al.*, 2004b] were identified as segments (6, 7, 10 and 12) [*Mendel et al.*, 1997]. These low-relief segments do not correspond to significant gravity anomalies and are therefore not inferred to have a thicker crust and

higher melt supply in their center [*Cannat et al.*, 1999]. Fresh looking volcanics are not observed in the two other low-relief segments (9 and 13), which instead display smooth nonvolcanic seafloor [*Cannat et al.*, 2006]. Segment 9 is part of an 82-km-long highly tectonized and sedimented section of the ridge (64°31′E–65°20′E) corresponding to positive gravity anomalies (inferred thinner crust) with upper mantle rocks exposed at the seafloor [*Mendel et al.*, 2003; *Sauter et al.*, 2004b]. Segment 13 belongs to a 100-km-long nonvolcanic ridge section (61°50′E–62°45′E) [*Cannat et al.*, 2006]. Such long nonvolcanic and tectonized ridge sections have also been described recently on the Gakkel Ridge [*Cochran et al.*, 2003; *Michael et*
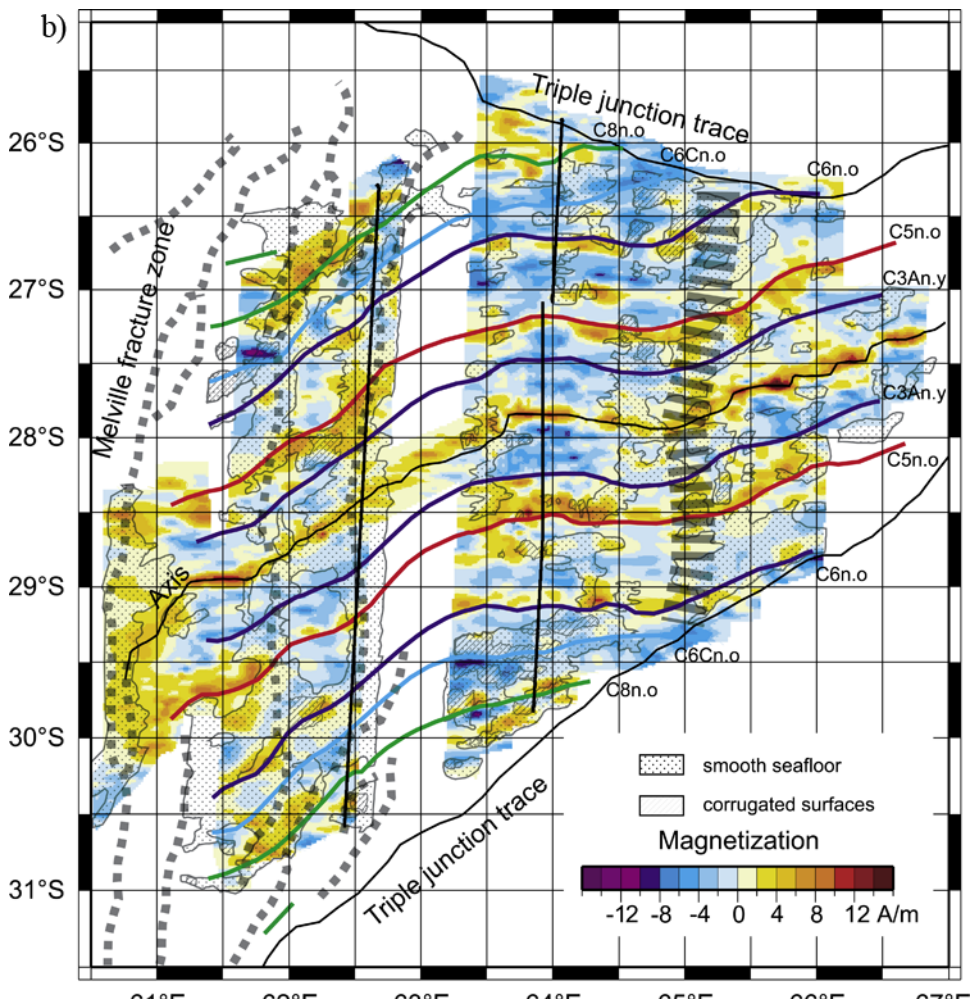
Figure 3. (continued)

al., 2003] and in the western most part of the SWIR as amagmatic accretionary ridge segments [*Dick et al.*, 2003].

[12] The axial valley strikes E-W, perpendicular to the spreading direction, along the three high-relief segments (8, 11 and 14). In the western part of the survey area, the axis is strongly oblique (N60°E) in the 220-km-long ridge section between segments 14 and 11 (Figure 2). This obliquity corresponds to an offset of 125 km in the spreading direction. The ridge turns at segment 11 and strikes N95°E subperpendicular to the spreading direction between segment 11 and 65°E. Right lateral minor offsets of 9 km and 6 km do not affect the overall trend of the axis in that central section. The axial valley becomes again oblique (N70°E) in the eastern part of the survey area with an en echelon setting of the E-W trending axial volcanic ridges of segments 8 and 6 (Figure 2). A nontransform discontinuity to

the west of segment 8 offsets the ridge by ~30 km and smaller offsets (<15 km) occur in the eastern most part of the survey area.

5.2. Off-Axis Segmentation

[13] The off-axis traces of present-day nontransform discontinuities between spreading segments 14, 13 and 12 are clearly marked in the off-axis bathymetric, gravimetric and magnetic records (Figures 1–3). They are revealed by two subparallel N5°E trending alignments of oblique basins (striking N60°E and up to 40 km long) with smooth seafloor. The axes of maximum depth of these alignments correlate well with isochron offsets and gravity highs (RMBA > 25 mGal) [*Cannat et al.*, 2006]. They bound bathymetric highs covered with volcanic seafloor and abyssal hills associated with elongated lower RMBA areas corresponding to the traces of segments 14 and 13. Both the off-axis traces

of the segments and the discontinuities extend from the axis to anomaly C6n.o (~20 Ma) and strike subparallel to the spreading direction, indicating the stability of the segmentation. Prior to anomaly C6Cn.o, when the spreading rate was two times higher, the shape of the discontinuities changes and the offsets between isochrons correspond to a series of narrow and deep troughs striking N20–25°E (Figure 1).

[14] By contrast, to the east of 63°E where the ridge trend is nearly orthogonal to spreading, the ridge flanks do not display clear traces of past axial segmentation in the central part of the survey area. The off-axis gravity low bull's-eyes appear heterogeneously distributed [*Cannat et al.*, 2006] and occur mostly in the African plate after magnetic anomaly C6n.o. Off-axis crustal thickness, as modeled from gravity anomalies, is on average larger in the northern than in the southern ridge flank, suggesting persistent tectonic asymmetry [*Cannat et al.*, 2006]. While there is no clear evidence for a long-lasting ridge segmentation pattern, there is a broad and slightly V-shaped region with mainly smooth seafloor, between 65° and 65°30′E, with on average higher RMBA (Figures 1 and 2). This V-shaped region, extends from the axis to the triple junction traces, and corresponds to the boundary between the central section where magnetic isochrons are nearly orthogonal to the spreading direction and an eastern domain with slightly oblique spreading (N70–60°E trending magnetic isochrons). The tip of this broad V-shaped region corresponds at the axis with the highly tectonized and sedimented ridge section between segment 11 and 8. We interpret the V-shaped region of mainly smooth seafloor as the off-axis trace of this present-day nonvolcanic ridge section.

6. Magnetic Structure of the Different Types of Seafloor

6.1. Axial Magnetization

[15] The variability in crustal magnetization was examined along the axis defined in the bathymetry, i.e., along the crest of the axial volcanic ridges when present and along the deepest point of the axial valley in portions of the axis with no resolvable volcanic features. As expected this bathymetric-defined axis runs along the maximum values of magnetization in the high-relief segments (Figure 3b) but, as the axial magnetization high may become poorly defined in the nonvolcanic sections of the ridge, we use a narrow 3-nm-wide strip of seafloor along the bathymetric-defined axis to get an averaged

value of the axial magnetization. The three high-relief segments (14, 11 and 8; Figure 4d) expose volcanic seafloor (Figure 4e), and correspond to gravity lows (Figure 4d) inferred to be due to thicker crust. These high-relief segments are also characterized by crustal magnetization values of 7 to 18 A/m higher than in the intervening areas of deeper and dominantly smooth seafloor (Figure 4c). Lower magnetizations have also been obtained for deeper parts of the axis, away from volcanic ridges, in other regions of the SWIR [*Dick et al.*, 2003; *Hosford et al.*, 2003; *Sauter et al.*, 2004a]. There is a signif- icant decrease (of up to 5 A/m) between crustal magnetization values averaged over the center of segments 8, 11 and 14 for the 3-nm-wide, and for a 7-nm-wide strip of axial seafloor (Figure 4c). The wider averaging window encompasses roughly the whole width of the axial valley floor up to the Brunhes/Matuyama reversal, and corresponds thus to crustal ages up to ~0.8 Ma. By contrast, sections of the axis with no resolvable volcanic features have a more constant magnetization over the width of the axial valley (Figure 4c).

[16] To determine whether intrinsic magnetization of the extrusive source layer can be responsible for the observed variations of axial crustal magnetization, we used the chemistry of basalts sampled on-axis in our study area [*Meyzen et al.*, 2003; *Robinson et al.*, 2001] to predict their magnetization with the empirical relationship developed by *Gee and Kent* [1998] between basalt FeO content and natural remanent magnetization (NRM). Predicted magnetization values (Figure 4c) are either within the range of crustal magnetization values derived from our magnetic inversion, or significantly higher (up to 21 A/m for iron-rich basalts from the distal regions of segments 11 and 14 that have crustal magnetization values <5 A/m).

[17] Figure 5 shows a wide range of RMBA (−20 to 30 mGal) and crustal magnetization (up to 18 A/m) values for axial seafloor with a volcanic morphology, contrasting with a more limited range of RMBA (15 to 35 mGal) and of magnetization values (<10 A/m) for axial seafloor with a smooth morphology. Both the mean magnetization and the standard deviation for volcanic seafloor are higher than those for nonvolcanic seafloor (Figure 5). There is a weak negative correlation between crustal magnetization and RMBA in volcanic seafloor, i.e., thinner crust has slightly lower magnetization, particularly for the youngest seafloor (Figure 5). This correlation (r = 0.54 for N = 1481 for the 3-nm-wide strip over the axis;
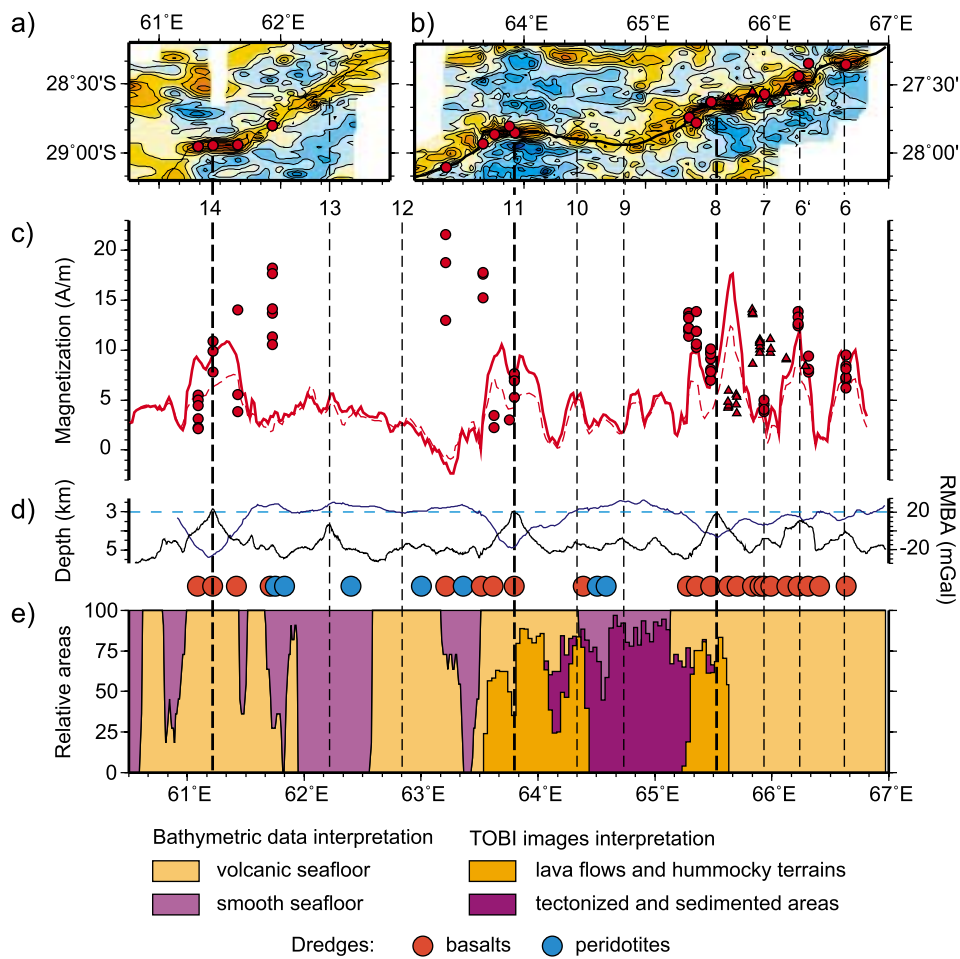
Figure 4. Along-axis variability of the magnetic structure. Figures 4a and 4b are details of the magnetization map (Figure 3b). Figure 4c shows along-axis variation in magnetization of the 500-m-thick model magnetic source layer. Vertical dashed lines correspond to the centers of segments 6 to 14. Thick red line: magnetization averaged along-axis over a 3-nm-wide strip; dashed red line: magnetization averaged along-axis over a 7-nm-wide strip (corresponding roughly to the axial valley inner floor up to the Brunhes/Matuyama reversal). Dots and triangles in Figure 4c are basalt magnetization values predicted from the FeO content of dredged basalts (located in Figures 4a and 4b) using the empirical relationship of *Gee and Kent* [1998] and major element concentrations given by *Robinson et al.* [2001] (triangles) and *Meyzen et al.* [2003] (dots). Figure 4d shows along-axis variations in axial depth (thick black line) and Residual Mantle Bouguer gravity Anomalies (RMBA, in blue). Figure 4e shows the along-axis distribution (in % of mapped area in the 7-nm-wide strip along the axis) of the smooth and volcanic seafloor morphologies, as observed on the bathymetric map [*Cannat et al.*, 2006], and of the volcanic and tectonized areas observed on TOBI images [*Sauter et al.*, 2004b]. The fit is good between these two distributions, TOBI-derived morphological analysis having a greater resolution. Dots above Figure 4e show the dominant lithologies observed during 5 manned submersible dives of the Shinkai 6500 during the "Indoyo" cruise [*Fujimoto et al.*, 1999] and found in dredges performed during the "Edul" cruise [*Mével et al.*, 1997; *Meyzen et al.*, 2003], the "Discovery 208" cruise [*Robinson et al.*, 2001], the "Atlantis II 093-5" cruise [*Price et al.*, 1986], and the "Antipode" cruise [*Mahoney et al.*, 1989]. Note that the volcanic and smooth seafloor areas correspond to dominantly basaltic and peridotitic seafloor, respectively.

Figure 5a) far exceeds the 1% chance that it is a random occurrence, and is thus statistically significant at the 99% confidence level. The residual gravity anomaly in volcanic seafloor thus predicts ~30% (i.e., 0.54^2) of the variation in axial magnetization, with other factors, such as noise, contrib-

uting the remaining ~70%. There is no such correlation for nonvolcanic seafloor. High-RMBA areas (>20 mGal) with a smooth seafloor display the same range of crustal magnetization values as high-RMBA areas with volcanic seafloor (Figure 5). Crustal magnetization of smooth seafloor crust is
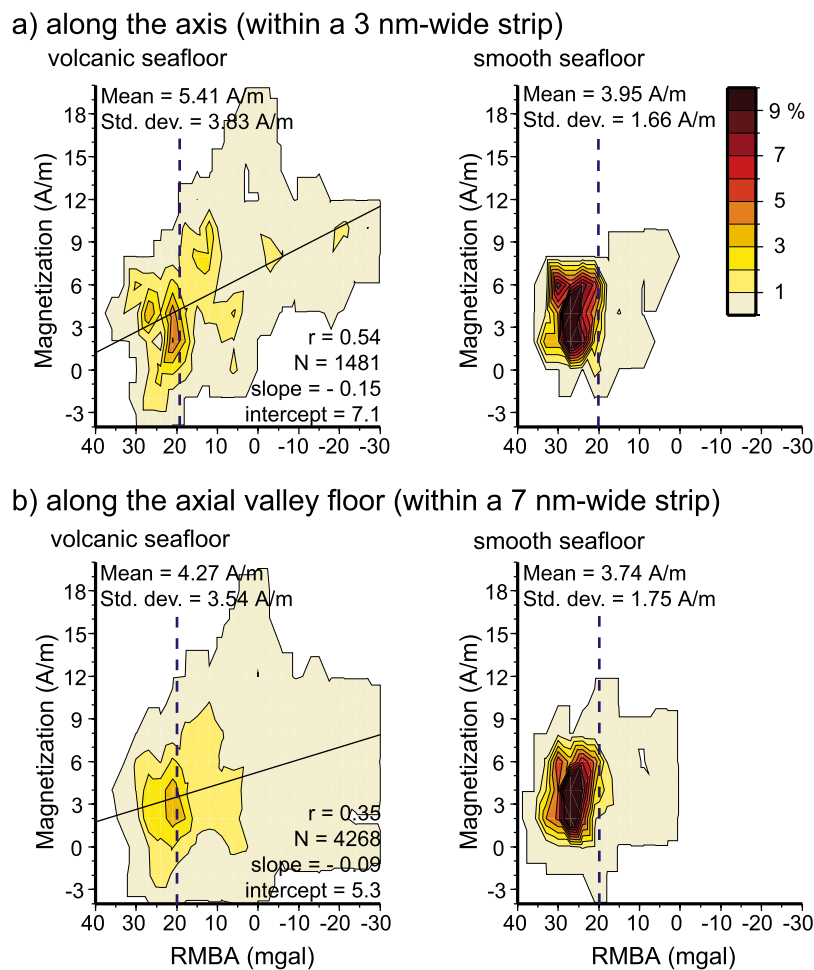
Figure 5. Bivariate density plots of crustal magnetization versus Residual Mantle Bouguer gravity Anomalies (RMBA) (a) sampled every 1 nm within a 3-nm-wide strip along the SWIR axis and (b) sampled every 1 nm within a 7-nm-wide strip corresponding roughly to the axial valley inner floor between 61°E and 67°E. The colors indicate the frequency of occurrence (in %) of each couple of values. The blue vertical line at 20 mGal is shown as reference.

highest (7 A/m) in the low-relief segments 9 and 13 (Figure 4c).

6.2. Off-Axis Magnetization

6.2.1. Amplitude of the Magnetic Anomalies

[18] Magnetic anomalies were identified along magnetic anomaly profiles almost everywhere in the survey area whatever the volcanic or nonvolcanic nature of the seafloor. We focus here on magnetic anomalies C5n and C6n which correspond to the two longest intervals of constant normal polarity (~1 Ma duration each) recorded in the survey area. The record of these chrons in sea-surface magnetic data is therefore less likely to suffer from contamination from adjacent magnetic

polarity blocks than would shorter polarity intervals [*Tivey and Tucholke*, 1998]. This lack of resolution in sea surface data due to the filtering effect of water depth and reversal spacing is of crucial importance in deep ultraslow spreading ridge sections as in our survey area. Identification of the anomalies C5n and C6n along magnetic anomaly profiles was easier in areas with more negative RMBA values (inferred thicker crust) and a volcanic seafloor. These areas have higher amplitude magnetic anomalies (e.g., 123 nT and 153 nT on average on volcanic seafloor for C6n and C5n, respectively) than areas with positive RMBA (inferred thinner crust) and a smooth seafloor (e.g., 81 nT and 137 nT on average on smooth seafloor for C6n and C5n, respectively). Smooth seafloor areas with the highest RMBA values (thinnest crust) located between 65° and 65°30′E
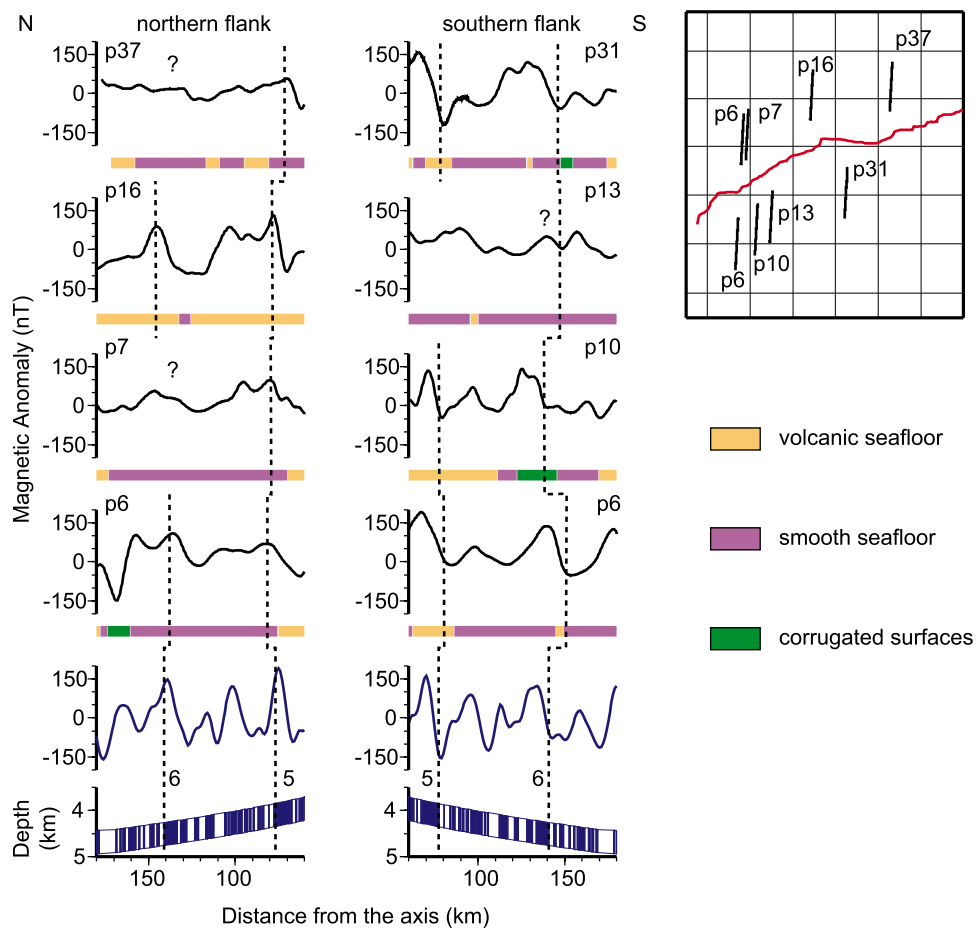
Figure 6. Representative magnetic anomaly profiles over corrugated surfaces and volcanic and smooth seafloor compared to a synthetic magnetic anomaly profile (bottom) calculated from a two-dimensional block model incorporating the calibrated magnetic inversion timescale of *Cande and Kent* [1995], with a 14 km/Ma spreading rate since 24 Ma and a 30 km/Ma spreading rate before, following *Patriat et al.* [2008].

are the only regions where C6n magnetic anomalies are too low for identification and picking to be performed. Figure 6 shows examples of shipboard magnetic profiles across magnetic anomalies C5n and C6n. Profiles p7 and p13 (Figure 6) illustrate the most common case: magnetic anomalies have lower amplitude over smooth seafloor. However, there are noticeable exceptions with large amplitude magnetic anomalies over smooth seafloor (e.g., profile p31 in Figure 6). Magnetic anomalies of profile p6 have larger amplitudes than those of profile p7 although both profiles are very close to one another and located over mostly smooth seafloor in the deep off-axis trace of the discontinuity between segment 14 and 13 where the RMBA is high. Well-marked magnetic anomalies are also observed over corrugated surfaces (e.g., profile p10 in Figure 6).

6.2.2. Local Standard Deviation of the Magnetization Map

[19] Magnetic anomalies thus appear best resolved, with the largest amplitudes, over the thicker crust (lower RMBA) volcanic seafloor domains. In order to further assess the capacity of the different types of seafloor to record magnetic anomalies, we estimate the local variability or "roughness" of the whole crustal magnetization map (Figure 3b). We calculated a directional local magnetic standard deviation perpendicular to the E-W isochrons. As we did not correct the magnetization grid for the polarity changes of the Earth's magnetic field, this directional standard deviation is related to the magnetization contrast between adjacent blocks of opposite polarity and may be thus interpreted as a proxy for the variation of the amplitude of the magnetic anomalies; a high local magnetic standard deviation indicating a well-marked magnetic
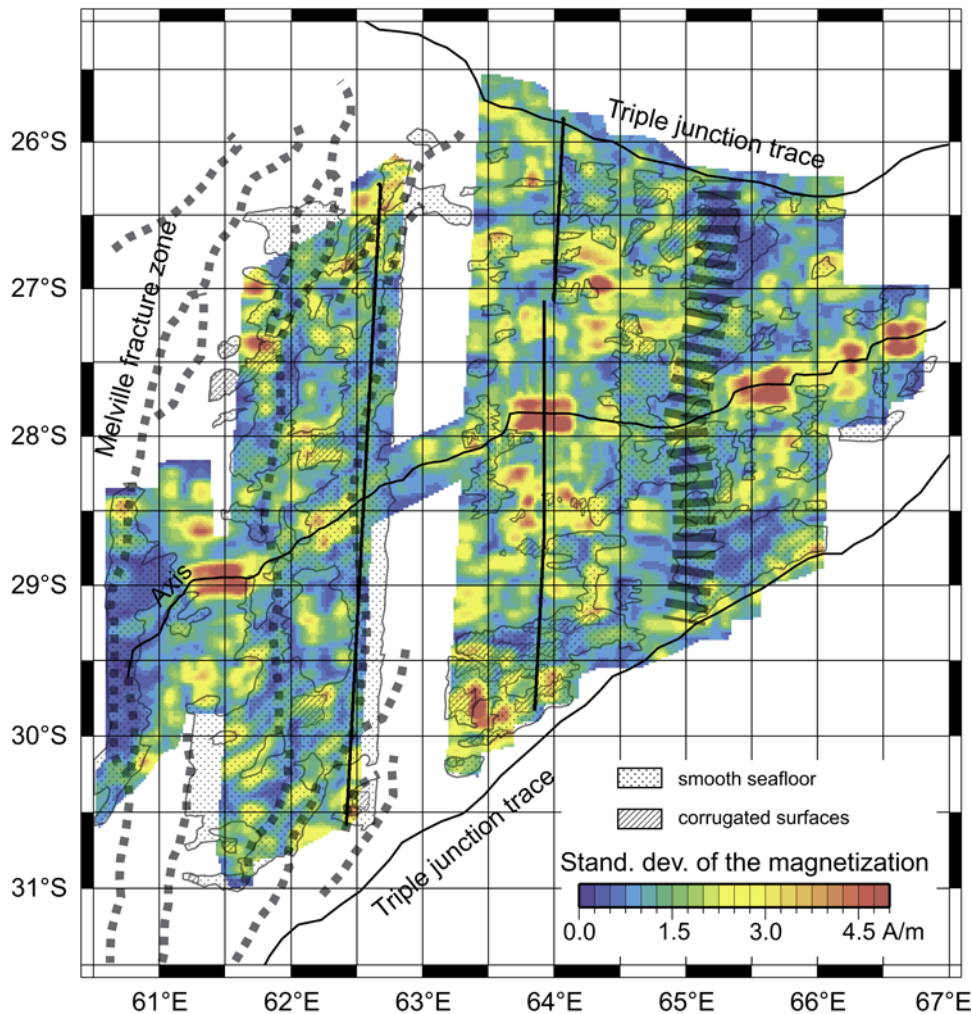
Figure 7. Standard deviation calculated at each point of the magnetization map using an elongated running window perpendicular to the E-W trending isochrons (11 nm long parallel to the N-S spreading direction and 1 nm wide). A high local standard deviation indicates a large magnetization contrast between adjacent blocks of opposite polarity and a well-marked magnetic anomaly. Magnetic standard deviations are maximum on-axis, over the center of segments 8, 11, and 14. By contrast, magnetic standard deviations are minimum in the deeper domains covered with smooth seafloor, both on-axis and off-axis.

anomaly. We focus again on the interpretation of the magnetization variability associated with the largest magnetic anomalies resulting from the longest intervals of constant polarity (e.g., C1, C5n, C6n...). We choose therefore a N-S and 11-nm-long window encompassing the largest magnetic anomalies. The computation is performed along each column of the magnetization grid (i.e., the window is as narrow as possible: 1 nm wide) to disregard the variability of the magnetization along the isochrons. Magnetic standard deviations are maximum on-axis, over the center of segments 8, 11 and 14 (Figure 7), where seafloor depths and

RMBA gravity anomalies are minimal (Figure 4). By contrast, magnetic standard deviations are minimum in the deeper domains covered with smooth seafloor, both on-axis and off-axis (Figure 7), where RMBA anomalies are higher. This confirms that thin crust nonvolcanic domains yield a poorer record of past inversions of the Earth's magnetic field. It must be noted, however, that the distributions of magnetic standard deviation values for volcanic and smooth seafloor domains have a very significant overlap and that the average standard deviation values differ by only 0.4 A/m (1.64 and 1.22 A/m for the volcanic and smooth seafloor
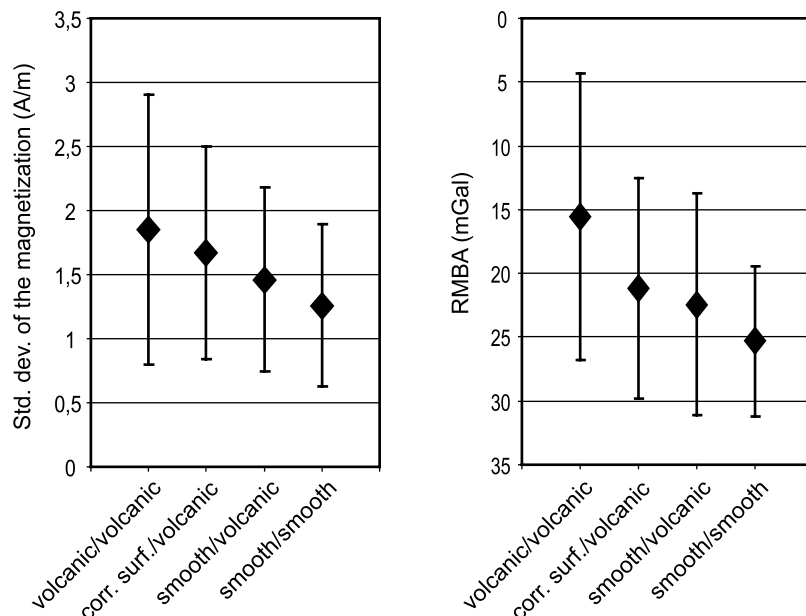
Figure 8. Comparison between seafloor morphology, standard deviation of the magnetization, and gravity signature using the grid of conjugate domains of *Cannat et al.* [2006]. Four types of conjugate pairs (volcanic-volcanic, corrugated-volcanic, smooth-volcanic, and smooth-smooth) inferred to have formed simultaneously on each side of the axial valley are plotted in order of decreasing standard deviation of the magnetization (or decreasing magnetic contrast) and increasing mean Residual Mantle Bouguer gravity Anomalies (RMBA) (or decreasing mean crustal thickness). Conjugate volcanic seafloor systematically has higher magnetization contrast and lower mean RMBA (or thicker crust), while conjugate smooth seafloor systematically has lower magnetization contrast and higher mean RMBA (or thinner crust).

domains, respectively). Comparing seafloor morphologies inferred to have formed simultaneously on each side of the axial valley [*Cannat et al.*, 2006] found that mean RMBA is lowest (i.e., inferred mean crustal thickness is maximum) for conjugate volcanic-volcanic seafloor domains, highest for conjugate smooth-smooth seafloor domains (i.e., inferred mean crustal thickness is minimum), and intermediate for conjugate corrugated-volcanic and smooth-volcanic seafloor domains (Figure 8). Although error bars are large, average values of the standard deviation of the crustal magnetization follow the same decreasing trend, indicating a decrease in the average capacity to provide a good record of past inversions of the Earth's magnetic field (Figure 8). Average magnetic standard deviation values are 1.85 A/m for conjugate volcanic-volcanic seafloor domains (standard deviation: 1.05 A/m), 1.67 A/m for conjugate corrugated-volcanic seafloor domains (standard deviation: 0.83 A/m), 1.46 A/m for conjugate smooth-volcanic seafloor domains (standard deviation: 0.72 A/m), and 1.26 A/m for conjugate smooth-smooth seafloor domains (standard deviation: 0.63 A/m).

6.2.3. Magnetization Variations Along C5n, C6n, C3r, and C5Br

[20] In order to further constrain the magnetic signature of the different types of seafloor, we analyzed crustal magnetization variations as a function of seafloor morphology for 4 long-lasting intervals of normal and reversed polarity (C5n, C6n and C3r, C5Br, respectively; Figure 9). The amplitude of off-axis along-isochron variations in crustal magnetization is significantly lower than the amplitude of on-axis variations calculated over a 3-nm-wide strip of seafloor (Figure 4c). It is, however, similar to the amplitude of on-axis variations calculated over a 7-nm-wide strip of seafloor (dashed line in Figure 4c).

[21] High crustal magnetization values (or highly negative magnetization in reverse polarity intervals) in the along-isochron off-axis profiles of Figure 9 commonly coincide with volcanic seafloor. This is, however, not systematically the case. Smooth seafloor locally has absolute crustal magnetization values up to 12 A/m, equal to the highest magnetization values for volcanic seafloor domains. High crustal magnetization is for example observed
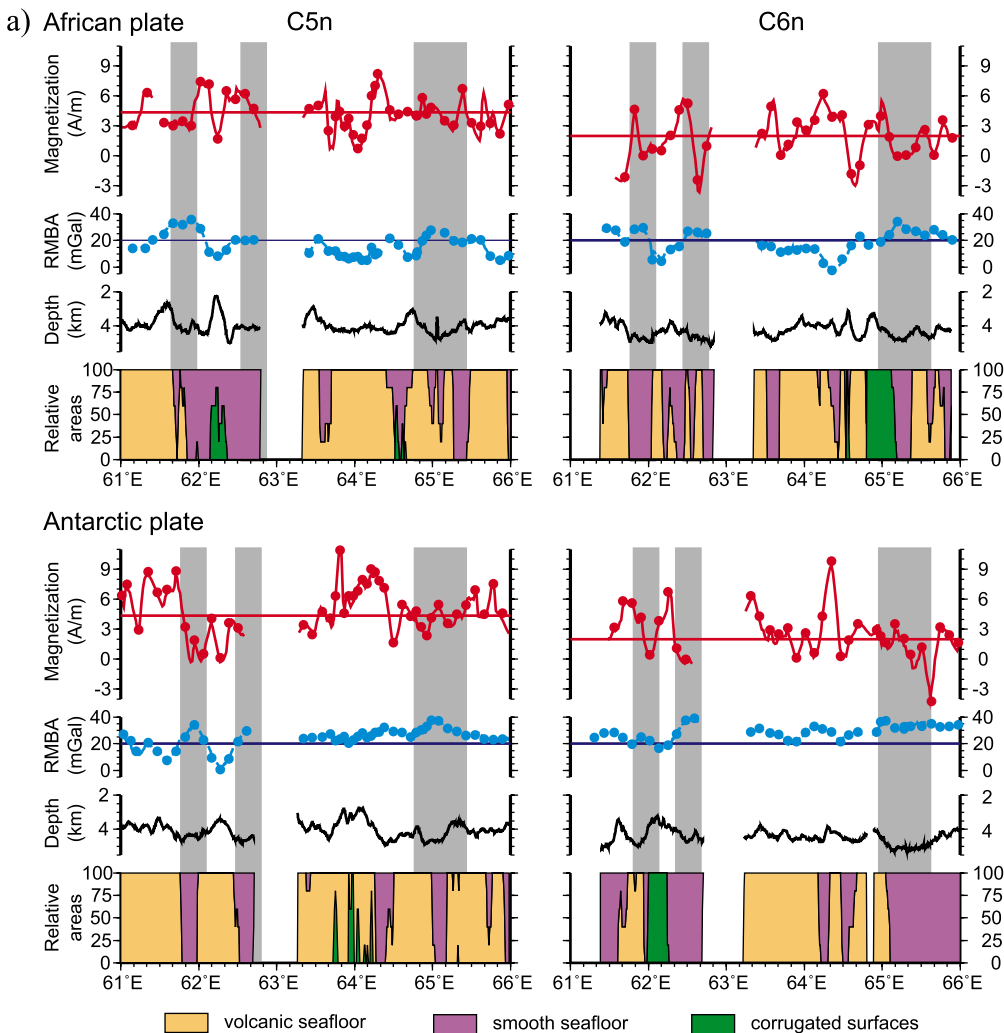
Figure 9. Magnetization values along (a) chrons C5n and C6n and (b) chrons C3r and C5Br compared to seafloor depth, Residual Mantle Bouguer gravity Anomalies (RMBA), and seafloor morphology (volcanic, smooth, or corrugated) in the African and Antarctic plates. Magnetization, seafloor depth, RMBA values, and the relative proportion of volcanic, smooth, and corrugated seafloor are averaged every 1 nm over a 3-nm-wide strip running along the magnetization peak of each magnetic anomaly (corresponding to the middle of the magnetic blocks). The red horizontal lines show the average magnetization value along the isochron. Filled circles along the RMBA and magnetization profiles indicate each isochron-crossing ship track. Note that the magnetization axis is reversed for the reversed polarity chrons. The blue horizontal line at 20 mGal is shown as reference and corresponds to inferred crustal thickness close to the reference value of 3.5 km [*Cannat et al.*, 2006]. Thick grey lines indicate the off-axis traces of the boundaries of segments 14 and 13 and the broad area of smooth nonvolcanic seafloor in the eastern ridge section.

over smooth seafloor at 62°30′E in chron C5n, and over corrugated and smooth seafloor between 62° and 63°E in chron C6n (Figure 9). Values of crustal magnetization are consistently low, however, in the off-axis traces of axial discontinuities (grey shaded domains in Figure 9). Along-isochron profiles for the reverse polarity chrons C3r and C5Br (Figure 9) tend to show a more coherent relation, similar to that observed in the on-axis profiles (Figure 4), between volcanic seafloor and higher crustal magnetization,

while smooth seafloor has lower crustal magnetization.

[22] In Figure 10, we compare the distribution of crustal magnetization values in volcanic seafloor and in smooth seafloor within chrons C5n, C6n, C3r and C5Br. Although these distributions are not statistically robust (the range of RMBA values and the proportion of volcanic and smooth seafloor considered for each chron are not identical), this
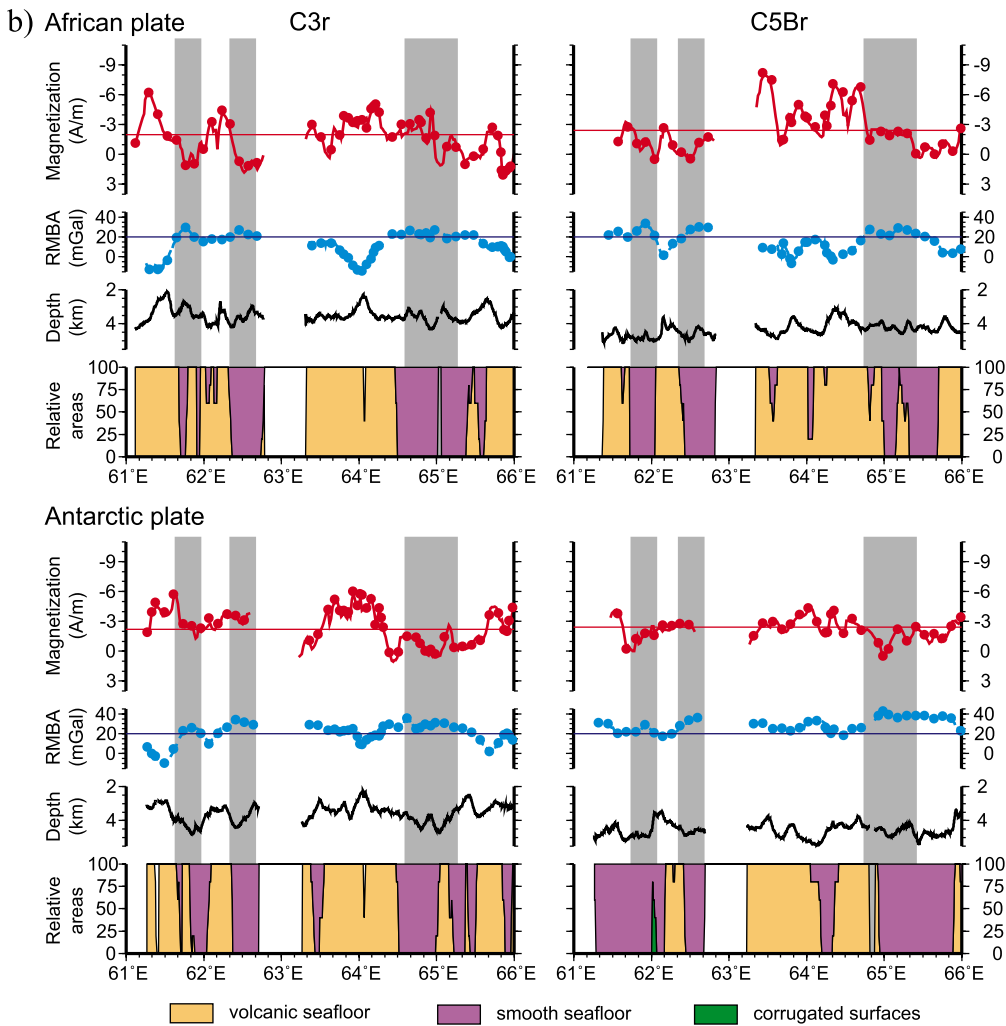
Figure 9. (continued)

comparison reveals differences between normal and reverse chrons. Let us consider first domains that have RMBA values lower than 20 mGal, which correspond to inferred crustal thickness greater than the reference crustal thickness used in gravity modeling (3.5 km [*Cannat et al.*, 2006]). Crustal magnetization values over these thicker crust areas tend to be higher over smooth than over volcanic seafloor in normal chrons (e.g., averaged magnetization is ∼3.8 and ∼1.8 A/m, respectively, for C6n; see Table 1 and A in Figure 10). This is not observed in reverse chrons. As a result, absolute crustal magnetization values averaged over the whole range of RMBA values are significantly lower for smooth seafloor than for volcanic seafloor in reverse chrons (e.g., averaged magnetization is ∼−1.2 and ∼−2.9 A/m, respectively, for C3r; see Table 1 and B in Figure 10), while they are similar in normal chrons (e.g., averaged magnetization is ∼4.3 and ∼4.6 A/m

for C5n; see Table 1 and C in Figure 10). Another difference is that crustal magnetization over domains that have RMBA values greater than 20 mGal (inferred thinner crust) spread to higher values (up to 12 A/m) in normal chrons than in reverse chrons (D in Figure 10). The magnetization distribution for the reverse polarity chron C5Br (Figure 10) is similar to that observed along the axis (Figure 5): magnetization values are higher over volcanic seafloor with RMBA values lower than 20 mGal (inferred thicker crust; E in Figure 10) than over volcanic seafloor with RMBA higher than 20 mGal (inferred thinner crust). There are also limited ranges of magnetization and RMBA values for seafloor with a smooth morphology along chron C5Br and C3r (F in Figure 10).

[23] Although this is not systematic, a clear shift to more positive crustal magnetization, regardless of polarity, is locally observed in smooth seafloor

areas. Figure 11 shows such an increase of the crustal magnetization for both the normal and the reversed magnetic chrons between the ridge axis and magnetic chron C3An near 64°30′E. Chron C2An and two adjacent reverse chrons (probably C2r and C2Ar) show more positive crustal magnetization values in the eastern areas with high RMBA and smooth seafloor (B in Figure 11) than
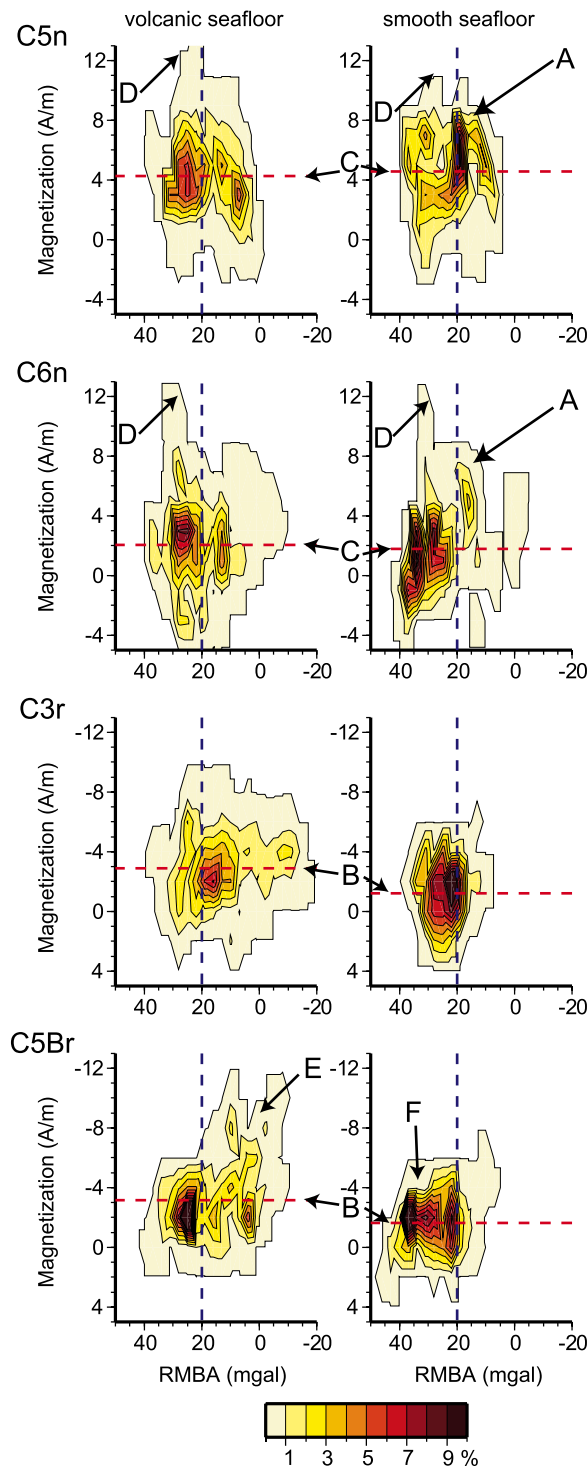
in the western low RMBA and volcanic areas (A in Figure 11): magnetization values are increasing eastward along C2An while they become less negative along the adjacent reverse chrons. A component of positive crustal magnetization superimposed over both the normal and the reverse polarity signal could also explain the difference we just described in Figure 10, between normal and reverse chrons for smooth seafloor with thicker than normal inferred crust. Such shifts to more positive crustal magnetization values were observed in a more systematic way near segment ends at the MAR [*Pariso et al.*, 1996; *Pockalny et al.*, 1995; *Tivey and Tucholke*, 1998], and at the SWIR between Atlantis II and Novara FZs [*Hosford et al.*, 2003].

7. Discussion

7.1. Axial Magnetization

[24] We observe significantly higher axial crustal magnetization values over the center of segments 8, 11 and 14 (Figures 4 and 5), where seafloor depths and RMBA gravity anomalies are minimal and where volcanic constructions are prominent, than in the deeper axial areas covered with smooth nonvolcanic seafloor. This is an argument for a dominant contribution of the extrusive part of the crust to the production of the axial magnetic signal. It should be noted that, contrary to what has been observed in many segments of the faster spreading MAR [*Ravilly et al.*, 1998], we do not observe higher axial magnetization values at segment ends.

[25] Basalt magnetization values predicted from their chemistry (Figure 4c) are consistent with crustal magnetization values obtained from the inversion of magnetic anomaly data for a 500-m-thick source layer. Predicted values are within the

Figure 10. Bivariate density plots of inverted magnetization versus Residual Mantle Bouguer gravity Anomalies (RMBA) for the areas covered with volcanic seafloor and smooth topography. The RMBA and magnetization values were sampled within a 3-nm-wide strip along isochrons C5n, C6n, C3r, and C5Br (note that the magnetization axis is reversed for C3r and C5Br). The colors indicate the frequency of occurrence (in %) of each couple of values. The blue vertical line at 20 mGal is shown as reference and corresponds to inferred crustal thickness close to the reference value of 3.5 km [*Cannat et al.*, 2006]. Horizontal dashed lines correspond to the average magnetization for each type of seafloor (see Table 1). A–F are labels used in the text.

Table 1. Mean and Standard Deviation of the Magnetization Over Volcanic and Smooth Seafloor for Areas of Inferred Thicker and Thinner Crust Than the Reference Crustal Thickness Used in Gravity Modeling[a]

	Volcanic Seafloor	Volcanic Seafloor (RMBA > 20 mGal)	Volcanic Seafloor (RMBA < 20 mGal)	Smooth Seafloor	Smooth Seafloor (RMBA > 20 mGal)	Smooth Seafloor (RMBA < 20 mGal)
C5n	4.25 A/m (2.07)	4.41 A/m (1.93)	4.04 A/m (2.21)	4.57 A/m (2.16)	4.28 A/m (2.23)	5.01 A/m (1.97)
C6n	2.03 A/m (2.64)	2.14 A/m (2.71)	1.83 A/m (2.48)	1.79 A/m (2.35)	1.4 A/m (2.21)	3.79 A/m (2.01)
C3r	−2.87 A/m (1.92)	−2.54 A/m (2.23)	−3.01 A/m (1.74)	−1.21 A/m (1.55)	−1.16 A/m (1.58)	−1.5 A/m (1.28)
C5Br	−3.14 A/m (1.96)	−2.47 A/m (0.94)	−3.76 A/m (2.41)	−1.62 A/m (1.24)	−1.59 A/m (1.2)	−1.99 A/m (1.58)

[a]Standard deviation is given in parentheses. The reference crustal thickness is 3.5 km [*Cannat et al.*, 2006]. The areas of inferred thicker and thinner crust have RMBA < 20 mGal and RMBA > 20 mGal, respectively.

range of crustal magnetization values for the center of segments 8, 11 and 14 (Figure 4c), suggesting that a 500-m-thick extrusive layer is indeed a reasonable hypothesis for the magnetic source there. By contrast, basalt magnetization values derived for the distal parts of segments 11 and 14 are much higher than crustal magnetization obtained from the inversion of magnetic anomalies (Figure 4c). This may indicate that the extrusive source layer in these distal parts is thinner than the 500 m used in the inversion. As a matter of fact, smooth seafloor morphologies in the distal western portion of segment 11 (Figure 4e) indicate that the extrusive layer there is absent, sampled basalts coming from volcanic plugs isolated in the axial valley floor [*Sauter et al.*, 2004b].

[26] It should be noted that basalt magnetization inferred from FeO contents correspond to maximum values, for unaltered lithologies sampled on pillow lavas and at the tops of lava flows. The interiors of massive flows commonly have lower NRM intensity than the tops of the flows because of different magnetic grain size distributions [*Zhou et al.*, 2001]. Moreover, although the low-temperature oxidation of the magnetic carriers in basalts may be a gradual long-term process [*Zhou et al.*, 2001], MORBs may become appreciably magnetically altered very early in their history [*Kent and Gee*, 1996]. Variations of the crustal magnetization in axial volcanic domains may thus also be due to variations of the intrinsic magnetization of the basaltic source layer, with age and increasing
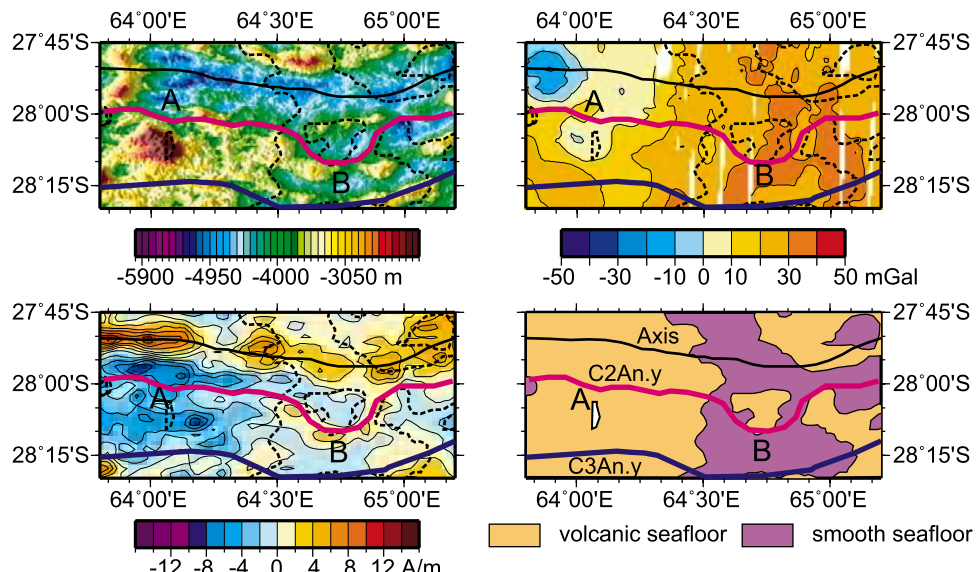
Figure 11. Bathymetric, Residual Mantle Bouguer gravity Anomalies (RMBA), magnetization, and seafloor morphology maps of the southern flank of the SWIR (63°40′E–65°10′E) between the axis and C3An.y. Dashed lines indicate the edges between the volcanic and smooth seafloor areas. Note, for the chrons between the axis and C3An (C2An in magenta and two adjacent reverse chrons, probably C2r and C2Ar), the eastward shift to more positive magnetization values from the western low RMBA and volcanic areas (area A) toward the eastern areas with high RMBA and smooth seafloor (area B).

low-temperature oxidative alteration [*Zhou et al.*, 2001]. This alteration effect may be enhanced in the distal parts of segments where fewer eruptions could result in on-average older seafloor, and where the effects of tectonic disruption may be greater [*Sauter et al.*, 2004a]. Other processes, such as geomagnetic intensity variations, are also contributing significantly to the rapid changes in the source layer magnetization from the ridge axis toward the flanks. The increase in geomagnetic intensity, from 40 ka to 3 ka [*Gee et al.*, 1996], is likely to cause the significant decrease between crustal magnetization values averaged over the center of segments 8, 11 and 14 for a narrow strip along the axis, and for the whole width of the axial valley floor up to ~0.8 Ma crustal ages.

[27] Thinning and alteration of a basaltic source layer may not, however, account for all along-axis variations in crustal magnetization shown in Figure 4c. Smooth seafloor axial domains, with no evidence for an extrusive upper crustal layer, have crustal magnetizations up to 6 A/m, and crustal magnetization values for volcanic seafloor at 63°E are lower than crustal magnetization values for smooth seafloor at 62° or at 65°E. This indicates that, although the basaltic source layer probably dominates the present-day along-axis magnetic signal, there may also be a contribution from the serpentinized peridotites that crop out in smooth seafloor areas [*Seyler et al.*, 2003], and possibly also a contribution from a deeper, gabbroic source. These contributions are discussed in the following section.

7.2. Off-Axis Magnetization

[28] Our analysis of the crustal magnetization map reveals that magnetization contrasts on and off-axis are on average higher for volcanic seafloor than for smooth topography (Figures 7 and 8). Areas with smooth seafloor also tend to correspond to lower crustal magnetization values (Figure 10). This suggests that the contribution of the basaltic upper crustal layer to the production of magnetic anomalies remains important in off-axis regions. However, the distribution of crustal magnetization in volcanic seafloor and smooth seafloor domains overlap broadly (Figure 10), and smooth seafloor or corrugated domains generally show reasonably good records of the geomagnetic polarity history (Figure 6). Furthermore, along-isochron variations of crustal magnetization show that smooth seafloor domains locally have higher crustal magnetization values over thick crust areas than volcanic seafloor domains (Figures 9 and 10). This supports the

hypothesis made in view of on-axis data, that basalts are not the only source of the magnetic anomaly record in our study area.

7.2.1. Contributions of Gabbros

[29] Gabbros are capable of carrying significant, stable remanent magnetization which is sufficient to account for sea-surface magnetic anomalies [*Pariso and Johnson*, 1993; *Worm*, 2001]. A 1.5-km-thick section of gabbroic crust with mean remanent intensities of 2.0–2.5 A/m and large Koenigsberger ratios has been drilled at ODP Hole 735B [*Kikawa and Pariso*, 1991; *Pariso and Johnson*, 1993; *Dick et al.*, 2000]. This drill hole is located along the Atlantis II transform fault, in a region of the SWIR where both the depth of the axis and the geochemical proxy for the extent of mantle melting (e.g., $Na_{8.0}$) indicate a higher magmatic budget than in our survey area. The uniform inclination of both fresh and altered rocks in Hole 735B suggests that the entire drilled section cooled below the Curie point for magnetite during a single polarity chron [*Kikawa and Pariso*, 1991] and does contribute to the magnetic anomaly observed above that section.

[30] Large Koenigsberger ratios of drill hole gabbros in Hole 735B [*Kikawa and Pariso*, 1991] provide strong evidence that these gabbros record a primary remanent magnetization component and that any induced component resides at a deeper level. A magnetic contribution of the whole lower crustal layer in our survey area would result in a strong negative correlation of decreasing crustal magnetization with increasing RMBA (assuming RMBA variations reveal only changes in crustal thickness). However, a negative correlation is barely recognizable between high RMBA and reduced magnetic contrast. Similar magnetization distributions for the northern flank with on average lower RMBA crust and for the southern flank with on average higher RMBA crust also confirm that there is no strong correlation between inferred crustal thickness and crustal magnetization.

[31] A synthetic magnetic anomaly profile calculated using a 1.5-km-thick upper layer of gabbros with a 2 A/m magnetization (a conservative estimate for the average effective magnetization of the entire crustal section at ODP Site 735 [*Pariso and Johnson*, 1993]) fits measured magnetic anomaly profiles collected over thick crust (low RMBA), volcanic seafloor domains of our study area. A synthetic model calculated using a 0.7-km-thick layer of altered basalt with a 3.5 A/m magnetization [*Johnson and Pariso*, 1993] also fits these
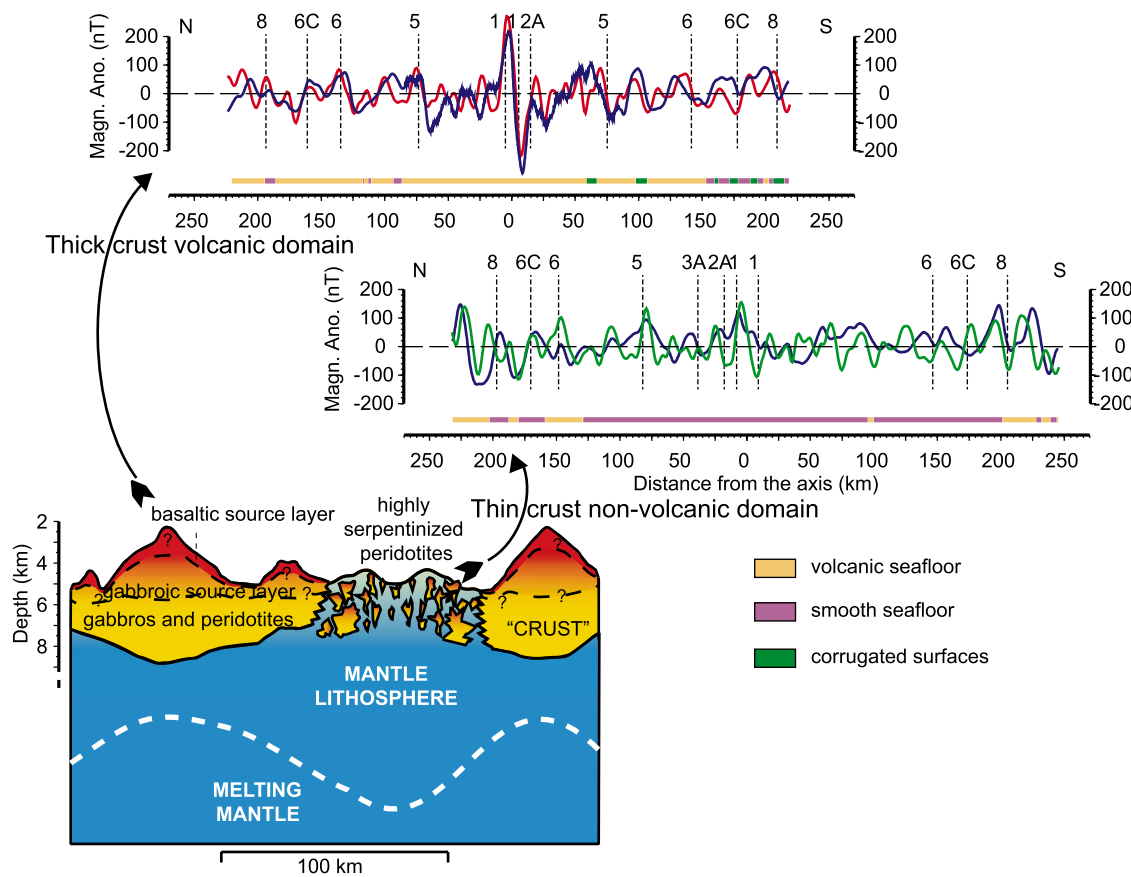
Figure 12. Sketch showing an along-axis idealized section of two magmatic segments separated by a magma-poor area. Two magnetic anomaly profiles illustrate the record of past inversions of the Earth's magnetic field (top) over a thick crust volcanic domain and (bottom) in a thinner crust, smooth seafloor domain. The profiles are located at about 64°E and 62°30′E, respectively, and are shown in Figures 1–3. The magnetic anomaly profile (in blue) collected in the volcanic domain is compared to a synthetic magnetic anomaly profile calculated using a 0.7-km-thick upper layer of altered basalt with a 3.5 A/m magnetization (in red). The magnetic anomaly profile (in blue) collected in the smooth seafloor domain is compared to a synthetic magnetic anomaly profile calculated using a 0.7-km-thick upper layer of serpentinized peridotites with a 4 A/m magnetization (in green). The effect of sloped polarity boundaries on magnetic anomaly amplitude has been modeled using the method of *Tisseau and Patriat* [1981] with a 0.7 contamination coefficient. The thickness of the crust in this sketch is derived from the gravity and seismic data [*Minshull et al.*, 2006]. The depth and shape of the lithosphere/asthenosphere boundary are unconstrained.

measured values (Figure 12). As basalts in the thick crust (low RMBA) volcanic areas contribute at least partly, 1.5 km should thus be considered as an upper bound for the thickness of such a deep magnetic source layer with a 2 A/m magnetization. We do not have strong constraints on the thickness of the extrusive layer in these domains, and possible variations of the intrinsic magnetization of basalts and gabbros are also not well constrained. Gabbroic samples of the MAR show juxtaposition of intervals of apparently normal and reversed polarity rocks over small spatial scales (less than a few meters) indicating an emplacement and/or cooling through successive polarity intervals [*Gee and Meurer*, 2002]. Shallowly inclined polarity

reversal boundaries within the lower oceanic crust have also been described on the SWIR [*Allerton and Tivey*, 2001]. The possibility of such multiple polarity reversal boundaries in a given vertical section can reduce significantly the overall effective magnetization of the gabbroic source layer. It therefore seems meaningless to go further into attempts to refine our forward modeling for thick crust volcanic domains.

[32] Gabbros represent only about 13% in weight of the rocks dredged in smooth seafloor domains of our study area, while serpentinized peridotites are the dominant lithologies [*Seyler et al.*, 2003]. Taking this relative amount of gabbros in the dredged rocks as typical for these smooth domains,

and a range of crustal thickness between 0.5 and 3 km (consistent with seismic and gravity-derived values in thin crust areas [*Cannat et al.*, 2006; *Minshull et al.*, 2006]) leads to a probable maximum thickness of gabbros of only 0.4 km in thin crust, smooth seafloor areas. This is consistent with the results of a wide-angle seismic experiment at 66°E which shows that thin crust domains have very thin, to absent Layer 3 (about 0.5 km at the most) [*Minshull et al.*, 2006]. Assuming a 2 A/m magnetization for gabbros, forward modeling shows that such a thin gabbroic layer cannot explain the magnetic anomaly profiles collected in high-RMBA areas with smooth seafloor. This would require a substantially thicker layer (about 1 km). Intrusions of Fe-Ti rich differentiated gabbros would have a higher magnetization (up to 16 A/m [*Pariso and Johnson*, 1993]) but may not occur in sufficient amounts. Moreover, the magnetization of Fe-Ti gabbros may be unstable [*Pariso and Johnson*, 1993]. Although our estimate of the maximum proportion of gabbros from dredge results is not robust, this suggests that we need an alternative source, besides gabbros, for the magnetic signal of smooth seafloor areas.

7.2.2. Contributions of Peridotites

[33] Serpentinized peridotites are serious candidates for this additional or alternative magnetic source. Studies of the magnetic properties of variably serpentinized peridotites [*Oufi et al.*, 2002; *Toft et al.*, 1990] show that their natural remanent magnetization can indeed be significant for high degrees of serpentinization (4–10 A/m on average for degrees of serpentinization greater than 75% [*Oufi et al.*, 2002]). These studies also show, however, that this natural remanent magnetization is highly variable. In particular, it depends on the distribution and size of magnetite grains produced during serpentinization, and on the iron content and abundance of secondary hydrous minerals such as brucite [*Oufi et al.*, 2002; *Toft et al.*, 1990]. Serpentinized peridotites are therefore versatile magnetic sources that may or may not produce strong signals depending on fluid-rock interactions and elemental exchanges that prevailed during serpentinization. Further support for significant remanent magnetization of ultramafic rocks is given by rotated paleomagnetic inclinations of serpentinized peridotites indicating substantial tectonic tilting on the MAR [*Garcés and Gee*, 2007]. In contrast to basalts and gabbros, serpentinized

peridotites can also have moderate to low Koenigsberger ratio and can therefore carry a significant component of induced magnetization [*Oufi et al.*, 2002].

[34] Forward modeling shows that a 0.5- to 0.7-km-thick layer of serpentinized peridotites with a 4 A/m magnetization can reproduce the magnetic anomalies measured over smooth seafloor areas (Figure 12). Wide-angle seismic data at 66°E reveal that thin crust domains have very thin to absent Layer 3, and a progressive gradient from upper crustal to mantle velocities [*Minshull et al.*, 2006]. This is similar to velocity profiles modeled over thin crust segment ends at the MAR and interpreted as due to an upward gradient of serpentinization in a crust composed mostly of mantle-derived ultramafic rocks [*Canales et al.*, 2000]. Assuming that this could also be the case in smooth seafloor domains of our study area, we used the P wave velocity structure modeled for 3-km-thick crust at 66°E [*Minshull et al.*, 2006] to calculate the maximum thickness over which degrees of serpentinization could be higher than 75% (Vp < 6 km/s [*Miller and Christensen*, 1997]). This leads to a 1.4-km-thick layer of highly serpentinized peridotites which could carry a remanent magnetic signal. Our forward modeling indicates that only half of this layer is enough to produce the magnetic anomalies observed in smooth seafloor areas (Figure 12).

[35] Highly magnetized serpentinized peridotites should also carry a component of induced magnetization. Serpentinized peridotites in the magnetic source have been proposed to account for shifts to more positive crustal magnetization values observed near segment ends at the MAR [*Pariso et al.*, 1996; *Pockalny et al.*, 1995; *Tivey and Tucholke*, 1998], and at the SWIR to the west of our study area [*Hosford et al.*, 2003]. We do observe a shift to more positive crustal magnetization values for smooth seafloor with moderate RMBA values (less than 20 mGal) in normal polarity chrons (A in Figure 10). We also observe a spread to more positive crustal magnetization values for both smooth seafloor domains and thin-crust (RMBA > 20 mGal) volcanic seafloor domains in normal polarity chrons (D in Figure 10). Such a spread to higher crustal magnetization values in normal polarity intervals would be expected for a source carrying a component of induced magnetization. Further evidence for induced magnetization is shown in Figure 11. We thus conclude that serpentinized peridotites, with both remanent and

induced magnetization, are likely carriers of the magnetic signal measured over smooth seafloor areas. However, smooth seafloor with high RMBA values (inferred thin crust), particularly in the deep off-axis traces of axial discontinuities, has weak absolute crustal magnetizations regardless of polarity (Figures 7–9). This could mean that exhumed mantle-derived peridotites there are not sufficiently serpentinized, or have undergone serpentinization in conditions that did not promote the formation of magnetite. A third possibility could be that magnetite there has been extensively altered.

[36] To summarize, we suggest that both gabbros, with a magnetization dominated by the remanent component [*Pariso et al.*, 1996], and highly serpentinized peridotites, carrying remanent and induced magnetizations [*Oufi et al.*, 2002], may contribute to magnetic anomalies in our survey area. The variable amplitude of magnetic anomalies in smooth seafloor areas may then be explained both by variable amounts of gabbros and highly serpentinized peridotites in the crust, and by variable conditions of serpentinization. Combined rock sampling and deep tow magnetics are now needed to address these uncertainties.

8. Conclusions

[37] The analysis of magnetic data along the Southwest Indian Ridge between 61°E and 67°E and their comparison with gravity data and the occurrence of volcanic and nonvolcanic seafloor types suggest the following conclusions:

[38] 1. At the ridge axis, the magnetic signal appears controlled mainly by variations of intrinsic magnetization and thickness of a layer of recent extrusive basalts. Axial crustal magnetization values are significantly higher over segment centers where seafloor depths and RMBA gravity anomalies are minimal and where volcanic constructions are prominent, than in the deeper axial areas covered with smooth nonvolcanic seafloor.

[39] 2. Off-axis, the amplitudes of magnetic anomalies C5n and C6n are on average higher over volcanic seafloor areas where thicker crust is inferred (low RMBA values) and lower over smooth nonvolcanic seafloor with inferred thinner crust (high RMBA values). Local standard deviation of the magnetization, a proxy for magnetization contrast, is on average higher for volcanic seafloor than for smooth nonvolcanic topography suggesting that the contribution of the basaltic

upper crustal layer to the production of magnetic anomalies remains important in off-axis regions.

[40] 3. However, the distribution of crustal magnetization in volcanic seafloor and smooth seafloor domains overlap broadly, and smooth seafloor or corrugated domains generally show reasonably good records of the geomagnetic polarity history. Furthermore, along isochron variations of crustal magnetization show that smooth seafloor domains locally have higher crustal magnetization values over thick crust areas than volcanic seafloor domains. This indicates that basalts are not the only source of the magnetic anomaly record in our study area.

[41] 4. Although the variations of the thickness and the intrinsic magnetization of gabbros are not well constrained, we infer from tentative two-dimensional forward models that an alternative source, besides gabbros, is needed to explain the magnetic signal of smooth nonvolcanic seafloor areas. An induced component of magnetization is present locally in some places with high RMBA values and smooth nonvolcanic seafloor but, it is not systematic and it is weak over most parts of the survey area. Serpentinized peridotites are likely carriers of this induced magnetization component. Both gabbros and serpentinized peridotites may thus contribute to the variable amplitude of magnetic anomalies measured over smooth nonvolcanic seafloor.

Acknowledgments

References

Allerton, S., and M. A. Tivey (2001), Magnetic polarity structure of the lower oceanic crust, *Geophys. Res. Lett.*, *28*(3), 423–426.

Canales, J. P., R. S. Detrick, J. Lin, J. A. Collins, and D. R. Toomey (2000), Crustal and upper mantle seismic structure beneath the rift mountains and across a non-transform offset at the Mid-Atlantic ridge (35°N), *J. Geophys. Res.*, *105*(B2), 2699–2719.

Cande, S. C., and D. V. Kent (1995), Revised calibration of the geomagnetic polarity timescale for the Late Cretaceous and Cenozoic, *J. Geophys. Res.*, *100*, 6093–6095.

Cann, J. R., D. K. Blackman, D. K. Smith, E. McAllister, B. Janssen, S. Mello, E. Avgerinos, A. R. Pascoe, and J. Escartín (1997), Corrugated slip surfaces formed at North Atlantic ridge-transform intersections, *Nature*, *385*, 329–332.

Cannat, M., C. Rommevaux-Jestin, D. Sauter, C. Deplus, and V. Mendel (1999), Formation of the axial relief at the very slow spreading Southwest Indian Ridge (49°–69°E), *J. Geophys. Res.*, *104*(B10), 22,825–22,843.

Cannat, M., C. Rommevaux-Jestin, and H. Fujimoto (2003), Melt supply variations to a magma-poor ultra-slow spreading ridge (Southwest Indian Ridge 61° to 69°E), *Geochem. Geophys. Geosyst.*, *4*(8), 9104, doi:10.1029/2002GC000480.

Cannat, M., D. Sauter, V. Mendel, E. Ruellan, K. Okino, J. Escartin, V. Combier, and M. Baala (2006), Modes of seafloor generation at a melt-poor ultraslow-spreading ridge, *Geology*, *34*(7), 605–608.

Cochran, J. R., G. J. Kurras, M. H. Edwards, and B. J. Coakley (2003), The Gakkel Ridge: Bathymetry, gravity anomalies, and crustal accretion at extremely slow spreading rates, *J. Geophys. Res.*, *108*(B2), 2116, doi:10.1029/2002JB001830.

Debayle, E., and J. J. Lévêque (1997), Upper mantle heterogeneities in the Indian Ocean from waveform inversions, *Geophys. Res. Lett.*, *24*, 245–248.

Dick, H. J. B., et al. (2000), A long in situ section of the lower oceanic crust: Results of ODP Leg 176 drilling at the Southwest Indian Ridge, *Earth Planet. Sci. Lett.*, *179*, 31–51.

Dick, H. J. B., J. Lin, and H. Schouten (2003), An ultraslow-spreading class of ocean ridge, *Nature*, *426*, 405–412.

Fujimoto, H., et al. (1999), First submersible investigations of mid-ocean ridges in the Indian Ocean, *InterRidge News*, *8*, 22–24.

Garcés, M., and J. S. Gee (2007), Paleomagnetic evidence of large footwall rotations associated with low-angle faults at the Mid-Atlantic Ridge, *Geology*, *35*(3), 279–282.

Gee, J., and D. V. Kent (1998), Magnetic telechemistry and magmatic segmentation on the southern East Pacific Rise, *Earth Planet. Sci. Lett.*, *164*, 379–385.

Gee, J., and W. P. Meurer (2002), Slow cooling of middle and lower oceanic crust inferred from multicomponent magnetizations of gabbroic rocks from the Mid-Atlantic Ridge south of the Kane fracture zone (MARK) area, *J. Geophys. Res.*, *107*(B7), 2137, doi:10.1029/2000JB000062.

Gee, J., D. A. Schneider, and D. V. Kent (1996), Marine magnetic anomalies as recorders of geomagnetic intensity variations, *Earth Planet. Sci. Lett.*, *144*, 327–335.

Harrison, C. G. A. (1987), Marine magnetic anomalies—The origin of the stripes, *Annu. Rev. Earth Planet. Sci.*, *15*, 505–543.

Horner-Johnson, B. C., R. G. Gordon, S. M. Cowles, and D. F. Argus (2005), The angular velocity of Nubia relative to Somalia and the location of the Nubia–Somalia–Antarctica triple junction, *Geophys. J. Int.*, *162*(1), 221–238.

Hosford, A., M. Tivey, T. Matsumoto, H. Dick, H. Schouten, and H. Kinoshita (2003), Crustal magnetization and accretion at the Southwest Indian Ridge near the Atlantis II fracture zone, 0–25 Ma, *J. Geophys. Res.*, *108*(B3), 2169, doi:10.1029/2001JB000604.

Johnson, H. P., and J. E. Pariso (1993), Variations in oceanic crustal magnetization: Systematic changes in the last 160 million years, *J. Geophys. Res.*, *98*(B1), 435–446.

Kent, D. V., and J. Gee (1996), Magnetic alteration of zero-age oceanic basalt, *Geology*, *24*, 703–706.

Kikawa, E., and J. E. Pariso (1991), Magnetic properties of gabbros from hole 735B, Southwest Indian Ridge, *Proc. Ocean Drill. Program Sci. Results*, *118*, 285–307.

Lagabrielle, Y., D. Bideau, M. Cannat, J. A. Karson, and C. Mével (1998), Ultramafic-mafic plutonic rock suites exposed along the Mid-Atlantic Ridge (10°N–30°N): Symmetrical-asymmetrical distribution and implications for seafloor spreading processes, in *Faulting and Magmatism at Mid-ocean Ridges*, *Geophys. Monogr. Ser.*, vol. 106, edited by W. R. Buck et al., pp. 153–176, AGU, Washington, D. C.

Lehnert, K., Y. Su, C. H. Langmuir, B. Sarbas, and U. Nohl (2000), A global geochemical database structure for rocks, *Geochem. Geophys. Geosyst.*, *1*(5), doi:10.1029/1999GC000026.

Lemaux, J., R. G. Gordon, and J. Y. Royer (2002), Location of the Nubia-Somalia boundary along the Southwest Indian Ridge, *Geology*, *30*(4), 339–342.

Macdonald, K. C., S. P. Miller, S. P. Huestis, and F. N. Spiess (1980), Three-dimensional modeling of a magnetic reversal boundary from inversion of deep-tow measurements, *J. Geophys. Res.*, *85*(B7), 3670–3680.

Mahoney, J. J., J. H. Natland, W. M. White, R. Poreda, S. H. Bloomer, R. L. Fisher, and A. N. Baxter (1989), Isotopic and geochemical provinces of the western Indian Ocean spreading centers, *J. Geophys. Res.*, *94*, 4033–4052.

Maus, S., et al. (2005), The 10th generation international geomagnetic reference field, *Phys. Earth Planet. Inter.*, *151*, 320–322.

Mendel, V., and D. Sauter (1997), Seamount volcanism at the super-slow spreading Southwest Indian Ridge between 57°E and 70°E, *Geology*, *25*(2), 99–102.

Mendel, V., D. Sauter, L. Parson, and J.-R. Vanney (1997), Segmentation and morphotectonic variations along a super-slow spreading center: The Southwest Indian Ridge (57°E–70°E), *Mar. Geophys. Res.*, *19*, 505–533.

Mendel, V., D. Sauter, C. Rommevaux-Jestin, P. Patriat, F. Lefebvre, and L. M. Parson (2003), Magmato-tectonic cyclicity at the ultra-slow spreading Southwest Indian Ridge: Evidence from variations of axial volcanic ridge morphology and abyssal hills pattern, *Geochem. Geophys. Geosyst.*, *4*(5), 9102, doi:10.1029/2002GC000417.

Mével, C., et al. (1997), Sampling the Southwest Indian Ridge: First results of the EDUL cruise (R/V Marion Dufresne II, August 1997), *InterRidge News*, *6*(2), 25–26.

Meyzen, C. M., M. J. Toplis, E. Humler, J. N. Ludden, and C. Mével (2003), A discontinuity in mantle composition beneath the southwest Indian ridge, *Nature*, *421*, 731–733.

Meyzen, C. M., J. N. Ludden, E. Humler, B. Luais, M. J. Toplis, C. Mével, and M. Storey (2005), New insights into the origin and distribution of the DUPAL isotope anomaly in the Indian Ocean mantle from MORB of the Southwest Indian Ridge, *Geochem. Geophys. Geosyst.*, *6*, Q11K11, doi:10.1029/2005GC000979.

Michael, P. J., et al. (2003), Magmatic and amagmatic seafloor generation at the ultraslow-spreading Gakkel ridge, Arctic Ocean, *Nature*, *423*(26), 956–962.

Miller, D. J., and N. I. Christensen (1997), Seismic velocities of lower crustal and upper mantle rocks from the slow-spreading mid-Atlantic ridge, south of the Kane Transform zone (MARK), *Proc. Ocean Drill. Program Sci. Results*, *153*, 437–454.

Minshull, T. A., M. R. Muller, and R. S. White (2006), Crustal structure of the Southwest Indian Ridge at 66°E: Seismic constraints, *Geophys. J. Int.*, *166*, 135–147.

Muller, M. R., T. A. Minshull, and R. S. White (1999), Segmentation and melt supply at the Southwest Indian Ridge, *Geology*, *27*(10), 867–870.

Munschy, M., and R. Schlich (1990), Etude géophysique des dorsales de l'océan Indien dans la région du point triple de Rodriguez, *Oceanol. Acta*, *10*, 119–128.

Nazarova, K. A. (1994), Serpentinized peridotites as a possible source for oceanic magnetic anomalies, *Mar. Geophys. Res.*, *16*(6), 455–462.

Okino, K., D. Curewitz, M. Asada, K. Tamaki, P. R. Vogt, and K. Crane (2002), Preliminary analysis of the Knipovich Ridge segmentation: Influence of focused magmatism and ridge obliquity on an ultraslow spreading system, *Earth Planet. Sci. Lett.*, *202*, 275–288.

Oufi, O., M. Cannat, and H. Horen (2002), Magnetic properties of variably serpentinized abyssal peridotites, *J. Geophys. Res.*, *107*(B5), 2095, doi:10.1029/2001JB000549.

Pariso, J. E., and H. P. Johnson (1993), Do layer 3 rocks make a significant contribution to marine magnetic anomalies? In situ magnetization of gabbros at Ocean Drilling Program hole 735 B, *J. Geophys. Res.*, *98*, 16,033–16,052.

Pariso, J. E., C. Rommevaux, and J. C. Sempéré (1996), Three-dimensional inversion of marine magnetic anomalies: Implications for crustal accretion along the Mid-Atlantic Ridge (28°–31°30′N), *Mar. Geophys. Res.*, *18*, 85–101.

Parker, R. L., and S. P. Huestis (1974), The inversion of magnetic anomalies in the presence of topography, *J. Geophys. Res.*, *79*, 1587–1593.

Patriat, P., D. Sauter, M. Munschy, and L. M. Parson (1997), A survey of the Southwest Indian Ridge axis between Atlantis II Fracture Zone and the Indian Triple Junction: Regional setting and large scale segmentation, *Mar. Geophys. Res.*, *19*, 457–480.

Patriat, P., H. Sloan, and D. Sauter (2008), From slow to ultra-slow: A previously undetected event at the Southwest Indian Ridge at ∼24 Ma, *Geology*, *36*(3), 207–210.

Pockalny, R. A., A. Smith, and P. Gente (1995), Spatial and temporal variability of crustal magnetization of a slowly spreading ridge: Mid-Atlantic ridge (20°–24°N), *Mar. Geophys. Res.*, *17*, 301–320.

Price, R. C., A. K. Kennedy, M. Riggs-Sneeringer, and F. A. Frey (1986), Geochemistry of basalts from the Indian Ocean triple junction: Implications for the generation and evolution of Indian Ocean ridge basalts, *Earth Planet. Sci. Lett.*, *78*, 379–396.

Ravilly, M., J. Dyment, P. Gente, and R. Thibaud (1998), Axial magnetic anomaly amplitude along the Mid-Atlantic Ridge between 20°N and 40°N, *J. Geophys. Res.*, *103*(B10), 24,201–24,221.

Robinson, C. J., M. J. Bickle, T. A. Minshull, R. S. White, and A. R. L. Nichols (2001), Low degree melting under the Southwest Indian Ridge: The roles of mantle temperature, conductive cooling and wet melting, *Earth Planet. Sci. Lett.*, *188*, 383–398.

Sauter, D., P. Patriat, C. Rommevaux-Jestin, M. Cannat, A. Briais, and G. S. a. S. Party (2001), The Southwest Indian Ridge between 49°15′E and 57°E: Focused accretion and magma redistribution, *Earth Planet. Sci. Lett.*, *192*, 303–317.

Sauter, D., L. M. Parson, V. Mendel, C. Rommevaux-Jestin, O. Gomez, A. Briais, C. Mével, K. Tamaki, and the FUJI Scientific Team (2002), TOBI sidescan sonar imagery of the very slow-spreading Southwest Indian Ridge: Evidence for along-axis magma distribution, *Earth Planet. Sci. Lett.*, *199*, 81–95.

Sauter, D., H. Carton, V. Mendel, M. Munschy, C. Rommevaux-Jestin, J.-J. Schott, and H. Whitechurch (2004a), Ridge segmentation and the magnetic structure of the Southwest Indian Ridge (at 50°30′E, 55°30′E and 66°20′E): Implications for magmatic processes at ultraslow-spreading centers, *Geochem. Geophys. Geosyst.*, *5*, Q05K08, doi:10.1029/2003GC000581.

Sauter, D., V. Mendel, C. Rommevaux-Jestin, L. M. Parson, H. Fujimoto, C. Mével, M. Cannat, and K. Tamaki (2004b), Focused magmatism versus amagmatic spreading along the ultra-slow spreading Southwest Indian Ridge: Evidence from TOBI side scan sonar imagery, *Geochem. Geophys. Geosyst.*, *5*, Q10K09, doi:10.1029/2004GC000738.

Seyler, M., M. Cannat, and C. Mével (2003), Evidence for major-element heterogeneity in the mantle source of abyssal peridotites from the Southwest Indian Ridge (52° to 68°E), *Geochem. Geophys. Geosyst.*, *4*(2), 9101, doi:10.1029/2002GC000305.

Smith, D. K., and J. R. Cann (1999), Constructing the upper crust of the Mid-Atlantic Ridge: A reinterpretation based on the Puna Ridge, Kilauea volcano, *J. Geophys. Res.*, *104*(B11), 25,379–25,399.

Smith, W. H., and D. T. Sandwell (1997), Global seafloor topography from satellite altimetry and ship depth soundings, *Science*, *227*, 1956–1962.

Smith, W. H. F., and P. Wessel (1990), Gridding with continuous curvature splines in tension, *Geophysics*, *55*, 293–295.

Tisseau, J., and P. Patriat (1981), Identification des anomalies magnétiques sur les dorsales à faible taux d'expansion: Méthode des taux fictifs, *Earth Planet. Sci. Lett.*, *52*, 381–396.

Tivey, M., and B. E. Tucholke (1998), Magnetization of 0–29 Ma ocean crust on the Mid-Atlantic Ridge, 25°30′ to 27°10′N, *J. Geophys. Res.*, *103*(B8), 17,807–17,826.

Toft, P. B., J. Arkani-Hamed, and S. E. Haggerty (1990), The effect of serpentinization on density and magnetic susceptibility: A petrological model, *Phys. Earth Planet. Inter.*, *65*, 137–157.

Tucholke, B. E., J. Lin, and M. C. Kleinrock (1998), Megamullions and mullion structure defining oceanic metamorphic core complexes on the Mid-Atlantic Ridge, *J. Geophys. Res.*, *103*(B5), 9857–9866.

Wang, X., and J. R. Cochran (1995), Along-axis gravity gradients at mid-ocean ridges: Implications for mantle flow and axial morphology, *Geology*, *23*(1), 29–32.

Wessel, P., and W. H. F. Smith (1995), New version of Generic Mapping Tools released, *Eos Trans. AGU*, *76*, 329.

Worm, H.-U. (2001), Magnetic stability of oceanic gabbros from ODP Hole 735B, *Earth Planet. Sci. Lett.*, *193*, 287–302.

Zhou, W., R. Van der Voo, D. R. Peacor, D. Wang, and Y. Zhang (2001), Low-temperature oxidation in MORB of titanomagnetite to titanomaghemite: A gradual process with implications for marine magnetic anomaly amplitudes, *J. Geophys. Res.*, *106*(B4), 6409–6421.